The Astrophysical Journal, 763:132 (16pp), 2013 February 1 doi:10.1088/0004-637X/763/2/132

INTENSITY MAPPING OF Lyα EMISSION DURING THE EPOCH OF REIONIZATION

Marta B. Silva[1,2], Mario G. Santos[1], Yan Gong[2], Asantha Cooray[2], and James Bock[3,4]
[1] CENTRA, Instituto Superior Técnico, Technical University of Lisbon, Lisboa 1049-001, Portugal
[2] Department of Physics & Astronomy, University of California, Irvine, CA 92697, USA
[3] Department of Physics, Mathematics and Astronomy, California Institute of Technology, Pasadena, CA 91125, USA
[4] Jet Propulsion Laboratory (JPL), National Aeronautics and Space Administration (NASA), Pasadena, CA 91109, USA
Received 2012 May 10; accepted 2012 November 30; published 2013 January 17

ABSTRACT

We calculate the absolute intensity and anisotropies of the Lyα radiation field present during the epoch of reionization. We consider emission from both galaxies and the intergalactic medium (IGM) and take into account the main contributions to the production of Lyα photons: recombinations, collisions, continuum emission from galaxies, and scattering of Ly*n* photons in the IGM. We find that the emission from individual galaxies dominates over the IGM with a total Lyα intensity (times frequency) of about (1.43–3.57) × 10^{-8} erg s^{-1} cm^{-2} sr^{-1} at a redshift of 7. This intensity level is low, so it is unlikely that the Lyα background during reionization can be established by an experiment aiming at an absolute background light measurement. Instead, we consider Lyα intensity mapping with the aim of measuring the anisotropy power spectrum that has rms fluctuations at the level of 1×10^{-16} [erg s^{-1} cm^{-2} sr^{-1}]^2 at a few Mpc scales. These anisotropies could be measured with a spectrometer at near-IR wavelengths from 0.9 to 1.4 μm with fields in the order of 0.5 to 1 deg^2. We recommend that existing ground-based programs using narrowband filters also pursue intensity fluctuations to study statistics on the spatial distribution of faint Lyα emitters. We also discuss the cross-correlation signal with 21 cm experiments that probe H I in the IGM during reionization. A dedicated sub-orbital or space-based Lyα intensity mapping experiment could provide a viable complimentary approach to probe reionization, when compared to 21 cm experiments, and is likely within experimental reach.

Key words: cosmology: theory – diffuse radiation – large-scale structure of universe

Online-only material: color figures

1. INTRODUCTION

The epoch of reionization (EoR) is a crucial stage in the history of galaxy formation, signaling the birth of the first luminous objects, during which the universe went from completely neutral to almost completely ionized (Barkana & Loeb 2001). This phase has been largely unexplored so far, although current observations suggest that it was reasonably extended (Komatsu et al. 2011; Fan et al. 2006) and a wide variety of observational avenues are being explored to probe it. In particular, the 21 cm line of neutral hydrogen is now understood to be a promising tool to study reionization and to understand the formation and evolution of galaxies during that epoch (see, e.g., Furlanetto et al. 2006). It is also now becoming clear that we need complimentary data in order to obtain extra insight into the sources of reionization. Such complimentary data could also aid in the interpretation of the H I signal by allowing ways to pursue cross-correlations and providing ways to reduce systematics and foregrounds encountered in 21 cm observations.

Recently, intensity mapping of other atomic and molecular lines at high redshifts, in particular CO and C II (Gong et al. 2011, 2012; Lidz et al. 2011; Visbal & Loeb 2010), has been proposed as a probe of reionization. In this work, we study the viability of also using intensity mapping of the Lyα line as an additional probe. For this study, we include several Lyα emission mechanisms involving both individual sources of emission such as galaxies and the emission and scattering associated with the intergalactic medium (IGM).

We consider both the integrated intensity and anisotropies of the Lyα line and suggest the latter as a new probe of reionization. In particular, we suggest that it will be possible to measure the amplitude of the Lyα intensity fluctuations with a narrowband spectrometer either from the ground with a suppression of atmospheric lines or from the orbital/sub-orbital platform.

The Lyα line, corresponding to transitions between the second and first energy level of the hydrogen atom, has a rest wavelength of approximately $\lambda_{Ly\alpha} = 1216$ Å. The signal present during reionization is observable in near-IR wavelengths today. Existing imaging observations made with narrowband filters on 10 m class telescopes focus on individual galaxy detections and are limited to a handful of narrow atmospheric windows at near-IR wavelengths. Given the strength of the line, it has now been seen in galaxies at $z \approx 6.98$ (Iye et al. 2006), $z \approx 8.2$ (Salvaterra et al. 2009), and $z \approx 8.6$ (Lehnert et al. 2010), reaching well into the EoR.

Deep narrowband surveys of high-redshift Lyα emitters have led to detections of a sufficient number of galaxies at redshifts 5.7, 6.6, 7.0, and 7.7 to allow constraints on the bright end of the Lyα luminosity function (LF) and its redshift evolution (e.g., Ouchi et al. 2008; Ota et al. 2010; Taniguchi et al. 2005; Iye et al. 2006; Shibuya et al. 2012). Observations of the Lyα LF indicate a decrease in the Lyα intensity from redshift 5.7 to 7.0. This would require a strong evolution of the Lyα emitter population, which is not predicted by most recent galaxy evolution models (Ota et al. 2010; Shibuya et al. 2012), or could be explained as the result of an increase in the fraction of IGM neutral hydrogen that would absorb or scatter Lyα photons from the observed galaxies (Haiman et al. 2000; Ota et al. 2008).

The scattering of Lyα photons by neutral hydrogen in the interstellar medium (ISM) and the IGM is expected to disperse the photons in both frequency and direction (Santos 2004). Such scattering could considerably decrease the Lyα intensity

per frequency bin from an individual galaxy, making the detection of most of the high-redshift galaxies impossible with current instruments. Exact calculations related to scattering are a difficult problem to solve analytically, and in simulations the scattering problem requires ray tracing of photons through the neutral medium in a simulation box (Zheng et al. 2010). While scattering makes individual galaxies dimmer, intensity mapping of the Lyα line at high redshifts can be an improvement over the usual experiments that make detections of Lyα emission from point sources and are only sensible to the strongest Lyα emitters. These are likely to be some of the brightest star-forming galaxies; however, any dust that is present in such galaxies, especially during the late stages of reionization, is likely to suppress the Lyα line. An experiment targeting the integrated emission will be able to measure all the sources of Lyα photons in a large region and will be sensitive to the extended, low surface brightness Lyα emission that is now known to generally form around star-forming regions (e.g., Steidel et al. 2011; Zheng et al. 2011). The anisotropy power spectrum of Lyα intensity then would be a probe of the Lyα halos around star-forming galaxies present during reionization. The cross-correlation with the 21 cm data could provide a direct test on the presence of neutral hydrogen in the extended Lyα halo.

The paper is organized as follows: In the next section we estimate the contribution to the Lyα emission from galaxies. In Section 3 we analyze the contributions to the Lyα emission from the IGM. In Section 4 we calculate the intensity of the Lyα signal, as well as its power spectrum, using a modified version of the code SimFast21 (Santos et al. 2010, 2011). In Section 5 we discuss the correlation of Lyα intensity maps with the 21 cm signal. Finally, in Section 6 we comment on the experimental feasibility of measuring the Lyα intensity power spectrum.

2. Lyα EMISSION FROM GALAXIES

The observed Lyα flux is mainly the result of line emission from hydrogen recombinations and collisional excitations in the interstellar clouds or in the IGM powered, respectively, by UV emission or UV and X-ray emission from galaxies. High-energy photons emitted by stars ionize hydrogen that then recombines to emit a rich spectrum of lines including an Lyα photon (Gould & Weinberg 1996; Fernandez & Komatsu 2006). Moreover, the electron ejected during this ionization heats the ISM or the IGM, increasing the probability of Lyα photon emission caused by collisional excitation (Gould & Weinberg 1996; Cantalupo et al. 2008). There is also a small contribution to the Lyα flux originated in the continuum emission from stars between the Lyα line and the Lyman limit (Chuzhoy & Zheng 2007; Barkana & Loeb 2005) plus Lyα from continuum free–free or free–bound emission, as well as two-photon emission during recombinations. This continuum will also make contributions to a given observation from lower redshifts besides the "Lyα" redshift (Cooray et al. 2012), which will confuse the Lyα signal. However, due to the smoothness of that continuum across frequency, we expect it should be possible to remove this contribution, for instance, by fitting a smooth polynomial in frequency for each pixel.

Another source of Lyα emission in the universe is cooling of gas that has suffered infall into a dark matter halo potential well. Several studies show that much of this cooling is made in the form of Lyα emission (Haiman et al. 2000; Fardal et al. 2001; Dijkstra et al. 2006a, 2006b; Dayal et al. 2010; Latif et al. 2011). Cold gas is used by galaxies as fuel to form stars, so there is a relation between the star formation rate (SFR) of a galaxy and the Lyα flux emitted as gas cools in that galaxy.

Since emission of Lyα radiation is closely connected with the star formation, the contribution from the several mechanisms by which Lyα radiation is emitted in galaxies and in the IGM can be related to the SFR of individual galaxies or galaxy samples. In order to calculate the emission of Lyα radiation from the IGM during the EoR, we also need to know the ionized fraction of hydrogen and the temperature of the gas in the IGM. Unfortunately, both these quantities are poorly constrained at $z \geqslant 6$ (Larson et al. 2011; Ouchi et al. 2010; Zahn et al. 2012). Since hydrogen ionization should be a consequence of stellar ionization/X-ray emission, we can in principle estimate it by following the SFR history and making sure that the resulting evolution of hydrogen ionized fraction is consistent with current constraints on the cosmic microwave background optical depth.

In order to obtain the SFR of galaxies at the high redshifts during the EoR, we make use of parameterizations that reproduce a correct reionization history. Our parameterizations are nonlinear in a similar way to the relations found in the Guo et al. (2011) and the De Lucia & Blaizot (2007) galaxy catalogs derived, respectively, from the high-resolution Millennium II (Boylan-Kolchin et al. 2009) and Millennium I (Springel et al. 2005) simulations. Such relations, when available from observations, make an improvement on the models instead of relying purely on theoretical calculations and semi-numerical simulations to predict all of the observations (Mesinger & Furlanetto 2007; Santos et al. 2010).

There are additional sources of radiation contributing to the Lyα emission, such as strong non-local sources of ionizing photons as expected from quasars, which would emit a large amount of energy in X-ray photons that would be able to ionize several neutral atoms, giving origin to a locally strong Lyα emission from recombinations. However, since the number of quasars is very small compared to the number of normal galaxies at the redshifts we are considering, we will neglect their contribution in the following calculations. We encourage future works on Lyα intensity to see if the shape of the power spectrum and other statistics can be used to choose between reionization histories that involve both galaxies and quasars.

In the following sub-sections we discuss in more detail the four processes for Lyα emission from galaxies: recombinations, excitations/relaxations, gas cooling, and photon emission from continuum processes.

2.1. Lyα Emission from Hydrogen Recombinations

Assuming ionizing equilibrium, the number of recombinations in galaxies is expected to match the number of ionizing photons that are absorbed in the galaxy and does not escape into the IGM. Depending on the temperature and density of the gas, a fraction of the radiation due to these recombinations is emitted in the Lyα line.

In the interstellar gas, most of the neutral hydrogen is in dense clouds with column densities greater than 3×10^{18} cm^{-2}. These clouds are optically thick to Lyα radiation, and Lyman photons are scattered in the galaxy several times before escaping into the IGM. Such multiple scatterings increase the probability of absorption. Assuming that these clouds are spherical and that the gas temperature is of the order of 10^4 K, Gould & Weinberg (1996) used atomic physics to study the probability of the Lyα emission per hydrogen recombination. They estimated that a fraction $f_{\rm rec} \approx 66\%$ of the hydrogen recombinations would result in the emission of an Lyα photon and that most of the other

recombinations would result in two-photon emission. These fractions should change with the temperature and the shape of the cloud, but such variations are expected to be small. Other calculations yield fractions between 62% and 68% according to the conditions in the cloud. In this paper we have chosen to use a value of $f_{\rm rec} = 66\%$ since the overall uncertainty on this number is lower than the uncertainty on the number of hydrogen recombinations.

The absorption of Lyα photons by dust is difficult to estimate and changes from galaxy to galaxy. Gould & Weinberg (1996) estimated that for a cloud with a column density $N \sim 10^{19}$ cm^{-2} the dust in the galaxy absorbs a fraction $f_{\rm dust} \approx 4\%$ of the emitted Lyα photons before they reach the galaxy virial radius; however, recent observations of high-redshift galaxies indicate a much higher $f_{\rm dust}$. In this study, we will use a redshift parameterization for the fraction of Lyα photons that are not absorbed by dust $f_{\rm Ly\alpha} = 1 - f_{\rm dust}$ that is double the value predicted by the study made by Hayes et al. (2011):

$$f_{\rm Ly\alpha}(z) = C_{\rm dust} \times 10^{-3}(1+z)^{\xi}, \quad (1)$$

where $C_{\rm dust} = 3.34$ and $\xi = 2.57$. The Hayes et al. (2011) parameterization was made so that $f_{\rm Ly\alpha}$ gives the difference between observed Lyα luminosities and Lyα luminosities scaled from SFRs assuming that the Lyα photons emitted in galaxies are only originated in recombinations. The high-redshift observations used to estimate $f_{\rm Ly\alpha}$ are only of massive stars, while the bulk of Lyα emission is originated in the low-mass stars that cannot be detected by current surveys. According to several studies (Forero-Romero et al. 2011), $f_{\rm Ly\alpha}$ decreases with halo mass, so it is possible that it is being underestimated in Hayes et al. (2011), which is why we decided to use a higher $f_{\rm Ly\alpha}$. Our results can, however, be easily scaled to other $f_{\rm dust}$ evolutions.

The number of Lyα photons emitted in a galaxy per second, $\dot{N}_{\rm Ly\alpha}$, that reach its virial radius is therefore given by

$$\dot{N}_{\rm Ly\alpha} = A_{\rm He} f_{\rm rec} \times f_{\rm Ly\alpha} \times (1 - f_{\rm esc}) \times \dot{N}_{\rm ion}, \quad (2)$$

where $A_{\rm He} = (4 - 4Y_p)/(4 - 3Y_p)$ accounts for the fraction of photons that go into the ionization of helium (Y_p is the mass fraction of helium), $\dot{N}_{\rm ion}$ is the rate of ionizing photons emitted by the stars in the galaxy, and $f_{\rm esc}$ is the fraction of ionizing photons that escape the galaxy into the IGM.

The ionizing photon escape fraction depends on conditions inside each galaxy and is difficult to estimate, especially at high redshifts. The precise determination of its value is one of the major goals of future observations of high-redshift galaxies at $z \gtrsim 7$. This parameter can be measured from deep imaging observations or can be estimated from the equivalent widths of the hydrogen and helium Balmer lines. The ionizing photon escape fraction dependence with the galaxy mass and the SFR, as a function of redshift, has been estimated using simulations that make several assumptions about the intensity of this radiation and its absorption in the ISM. However, for the halo virial mass range, 10^8–10^{13} $M_\odot$, and during the broad redshift range related to the EoR, there are no simulations that cover the full parameter space. Moreover, the limited simulations that exist do not always agree with each other (Gnedin et al. 2008; Wise & Cen 2009; Fernández-Soto et al. 2003; Siana et al. 2007; Haardt & Madau 2012). Razoumov & Sommer-Larsen (2010) computed the escape fraction of UV radiation for the redshift interval $z = 4$ to $z = 10$ and for halos of masses from $10^{7.8}$ to $10^{11.5}$ $M_\odot$ using a high-resolution set of galaxies. Their simulations cover most of the parameter space needed for reionization-related calculations, and their escape fraction parameterization is compatible with most of the current observational results. Thus, we use it for our calculations here.

Table 1
Fits to the Escape Fraction of UV Radiation from Galaxies as a Function of Redshift (based on Razoumov & Sommer-Larsen 2010)

z	α	β	$f_{\rm esc}(M = 10^{10}\,M_\odot)$
10.4	2.78×10^{-2}	0.105	0.732
8.2	1.30×10^{-2}	0.179	0.449
6.7	5.18×10^{-3}	0.244	0.240
5.7	3.42×10^{-3}	0.262	0.240

According to Razoumov & Sommer-Larsen (2010) simulations, the escape fraction of ionizing radiation can be parameterized as

$$f_{\rm esc}(M, z) = \exp[-\alpha(z) M^{\beta(z)}], \quad (3)$$

where M is the halo mass and α and β are functions of redshift (Table 1).

The number of ionizing photons emitted by the stars in a galaxy depends on its SFR, metallicity, and the stellar initial mass function (IMF). Making reasonable assumptions for these quantities, we will now estimate $\dot{N}_{\rm ion}$. Since this UV emission is dominated by massive, short-lived stars, we can assume that the intensity of ionizing photons emitted by a galaxy is proportional to its SFR. In terms of the SFR in one galaxy,

$$\dot{N}_{\rm ion} = Q_{\rm ion} \times {\rm SFR}, \quad (4)$$

where $Q_{\rm ion}$ is the average number of ionizing photons emitted per solar mass of star formation. This can be calculated through

$$Q_{\rm ion} = \frac{\int_{M_{\rm min}}^{M_{\rm max}} \Psi(M) Q_\star(M) t_\star(M) dM}{\int_{M_{\rm min}}^{M_{\rm max}} \Psi(M) M dM}, \quad (5)$$

where $\Psi(M) = K M^{-\alpha}$ is the stellar IMF, K is a constant normalization factor, and α is the slope of the IMF. In our calculation, we used a Salpeter IMF, with $\alpha = 2.35$. $t_\star(M)$ is the star lifetime and $Q_\star(M)$ its number of ionizing photons emitted per unit time. The values of $Q_\star$ and $t_\star$ were calculated with the ionizing fluxes obtained by Schaerer (2002) using realistic models of stellar populations and non-LTE atmospheric models, appropriated for Pop II stars with a $Z_\star = 0.02\,Z_\odot$ metallicity.

Assuming that ionizing photons are only emitted by massive OB stars sets a low mass effective limit for the mass of stars contributing to the UV radiation field of a galaxy. This limit is a necessary condition for the star to be able to produce a significant number of ionizing photons. For the stellar population used for this work we take $M_{\rm min} \approx 7\,M_\odot$ (Schaerer 2002; Shull et al. 2012). The integration upper limit is taken to be $M_{\rm max} = 150\,M_\odot$. In this paper, we calculated $Q_{\rm ion}$ using the parameterization values published in Schaerer (2002). The number of ionizing photons per second emitted by a star as a function of its mass is given by

$$\log_{10}[Q_\star/{\rm s}^{-1}] = 27.80 + 30.68x - 14.80x^2 + 2.5x^3 \text{ for } 7\,M_\odot < M_\star < 150\,M_\odot, \quad (6)$$

where $x = \log_{10}(M_\star/M_\odot)$ and the star's lifetime in years is given by

$$\log_{10}[t_\star/{\rm yr}] = 9.59\text{–}2.79x + 0.63x^2. \quad (7)$$

The use of these parameters results in $Q_{\rm ion} \approx 5.38 \times 10^{60}\, M_{\odot}^{-1}$. Shull et al. (2012) suggest the use of a different model for stellar atmosphere and evolution (R. S. Sutherland & J. M. Shull, unpublished) that yields $Q_{\rm ion} \approx 3.97 \times 10^{60}\, M_{\odot}^{-1}$. This may imply that the stellar emissivity we calculated is an overestimation and that consequently our Lyα flux powered by stellar emission may be overestimated by about 35%. This is comparable to other large uncertainties, such as the ones in the parameters $f_{\rm esc}$ and $f_{\rm dust}$. The Lyα luminosity is calculated assuming that the Lyα photons are emitted at the Lyα rest frequency, $\nu_0 = 2.47 \times 10^{15}$ Hz with an energy of $E_{{\rm Ly}\alpha} = 1.637 \times 10^{-11}$ erg. To proceed, we will assume that the SFR for a given galaxy is only a function of redshift and the mass of the dark halo associated with that galaxy. The Lyα luminosity due to recombinations in the ISM, $L_{\rm rec}^{\rm GAL}$, can then be parameterized as a function of halo mass and redshift as

$$L_{\rm rec}^{\rm GAL}(M,z) = E_{{\rm Ly}\alpha}\dot{N}_{{\rm Ly}\alpha} \approx 1.55 \times 10^{42}\,[1 - f_{\rm esc}(M,z)]\, f_{{\rm Ly}\alpha}(z) \times \frac{{\rm SFR}(M,z)}{M_{\odot}\ {\rm yr}^{-1}}\ {\rm erg\ s}^{-1}. \quad (8)$$

2.2. Lyα Emission from Excitations/Relaxations

The kinetic energy of the electron ejected during the hydrogen ionization heats the gas, and assuming thermal equilibrium, this heat is emitted as radiation. Using atomic physics, Gould & Weinberg (1996) estimated that for a cloud with a hydrogen column density of $\approx 10^{19}$ cm^{-2}, the energy emitted in the form of Lyα photons is about 60% for ionizing photons with energy $E_{\nu_{\rm lim}} < E_{\nu} < 4E_{\nu_{\rm lim}}$ and $\approx$50% for photons with energy $E_{\nu} > 4E_{\nu_{\rm lim}}$, where $E_{\nu_{\rm lim}} = 13.6$ eV is the Rydberg energy. The remaining energy is emitted in other lines.

Using the spectral energy distribution (SED) of galaxies with a metallicity $Z = 0.02\, Z_{\odot}$ from the code of Maraston (2005), we estimated that the average ionizing photon energy is $E_{\nu} = 21.4$ eV and that more than 99% of the photons have an energy lower than $4E_{\nu_{\rm lim}}$. According to the Gould & Weinberg (1996) calculation, the fraction of energy of the UV photon that is emitted as Lyα radiation due to the collisional excitations/relaxations is given by

$$E_{\rm exc}/E_{\nu} \sim 0.08 + 0.1\left(1 - \frac{2\nu_{\rm lim}}{\nu}\right) \sim 0.1. \quad (9)$$

For a cloud with the properties considered here this yields an energy in Lyα per ionizing photon of $E_{\rm exc} \approx 2.14$ eV or 3.43×10^{-12} erg. This results in an average of 0.16 Lyα photons per ionizing photon.

Finally, the Lyα luminosity due to excitations in the ISM, $L_{\rm exc}^{\rm GAL}$, is then

$$L_{\rm exc}^{\rm GAL}(M,z) = [1 - f_{\rm esc}(M,z)] f_{{\rm Ly}\alpha}(z) A_{\rm He}\dot{N}_{\rm ion}E_{\rm exc} \approx 4.03 \times 10^{41}\,[1 - f_{\rm esc}(M,z)]\, f_{{\rm Ly}\alpha}(z) \times \frac{{\rm SFR}(M,z)}{M_{\odot}\ {\rm yr}^{-1}}\ {\rm erg\ s}^{-1}, \quad (10)$$

where again it is assumed to be a function of the SFR.

2.3. Lyα Emission from Gas Cooling

During the formation of galaxies, gas from the IGM falls into potential wells composed mainly by dark matter that collapsed under its own gravity. The increase in the gas density leads to a high rate of atomic collisions that heat the gas to a high temperature. According to the study of Fardal et al. (2001), most of the gas in potential wells that collapses under its own gravity never reaches its virial temperature, and so a large fraction of the potential energy is released by line emission induced by collisions and excitations from gas with temperatures $T_K < 2 \times 10^4$ K. At this temperature approximately 50% of the energy is emitted in Lyα alone.

From Fardal et al. (2001), we can relate the luminosity at the Lyα frequency due to the cooling in galaxies to their baryonic cold mass, $M_{\rm cool}^{\rm bar}$, using

$$\log_{10}\left(L_{\rm cool}^{\rm GAL}\right) = 1.52\log_{10}\left(M_{\rm cool}^{\rm bar}\right) + 26.32, \quad (11)$$

where both the luminosity and the mass are in solar units. To relate this baryonic cold mass to a quantity we can use in our models, we used the relation between cold baryonic mass and the halo mass from the galaxies in the Guo et al. (2011) catalog. From the equation above, we can then obtain an expression for the luminosity, which can be fitted by

$$L_{\rm cool}^{\rm GAL}(M) \approx 1.69 \times 10^{35} f_{{\rm Ly}\alpha}(z)\left(1 + \frac{M}{10^8}\right) \times \left(1 + \frac{M}{2 \times 10^{10}}\right)^{2.1}\left(1 + \frac{M}{3 \times 10^{11}}\right)^{-3}\ {\rm erg\ s}^{-1}, \quad (12)$$

with M in units of $M_{\odot}$. The relation between the cold gas mass and the mass of the halo shows very little evolution with redshift during reionization. Thus, we expect the relation in Equation (13) to only depend on redshift due to the redshift evolution of $f_{{\rm Ly}\alpha}$.

2.4. Contributions from Continuum Emission

Continuum emission can also contribute to the Lyα observations. These include stellar emission, free–free emission, free–bound emission, and two-photon emission. Photons emitted with frequencies close to the Lyn lines should scatter within the ISM and eventually get re-emitted out of the galaxy as Lyα photons. Otherwise, they will escape the ISM before redshifting into one of the Lyn lines and being reabsorbed by a hydrogen atom.

The fraction of photons that scatter in the galaxy can be estimated from the intrinsic width of the Lyα line, which has $\approx$4 Å (Jensen et al. 2013). We calculated the stellar contribution assuming an emission spectrum for stars with a metallicity of $Z_{\star} = 0.02\, Z_{\odot}$ estimated with the code from Maraston (2005) that can be approximated by the emission of a blackbody with a temperature of 6.0×10^4 K for $h\nu < 13.6$ eV. The number of stellar origin Lyα photons per solar mass in star formation obtained with this method is

$$Q_{{\rm Ly}\alpha}^{\rm stellar} = 4.307\int_{\nu_{{\rm Ly}\alpha+2\,\text{Å}}}^{\nu_{{\rm Ly}\alpha-2\,\text{Å}}} d\nu \frac{\nu^3}{e^{h\nu/K_b T_K} - 1} M_{\odot}^{-1} = 9.92 \times 10^{58}\, M_{\odot}^{-1}. \quad (13)$$

We note that we are not accounting for the higher opacity at the center of the Lyα line, which should push the photons out of the line center before exiting the star, and so we may be overestimating the stellar Lyα photon emission.

Free–bound emission and free–free emission are, respectively, originated when free electrons scatter off ions with or without being captured. Following the approach of Fernandez & Komatsu (2006), the free–free and free–bound continuum luminosity can be obtained using

$$L_\nu(M, z) = V_{\rm sphere}(M, z)\varepsilon_\nu, \quad (14)$$

where $V_{\rm sphere}$ is the volume of the Strömgren sphere, which can be roughly estimated using the ratio between the number of ionizing photons emitted and the number density of recombinations in the ionized volume,

$$V_{\rm sphere}(M, z) = \frac{Q_{\rm ion}{\rm SFR}(M, z)(1 - f_{\rm esc})}{n_e n_p \alpha_\beta}. \quad (15)$$

Here ε_ν is the total volume emissivity of free–free and free–bound emission, n_p is the number density of protons (ionized atoms), and α_i is the case A or case B recombination coefficient (see Furlanetto et al. 2006).

The volume emissivity estimated by Dopita & Sutherland (2003) is given by

$$\varepsilon_\nu = 4\pi n_e n_p \gamma_c \frac{e^{-h\nu/kT_K}}{T_K^{1/2}}\ {\rm J\ cm^{-3}\ s^{-1}\ Hz^{-1}}, \quad (16)$$

where γ_c is the continuum emission coefficient including free–free and free–bound emission given in SI units by

$$\gamma_c = 5.44 \times 10^{-46}\left[\bar{g}_{\rm ff} + \Sigma_{n=n'}^{\infty}\frac{x_n e^{x_n}}{n} g_{\rm fb}(n)\right]. \quad (17)$$

Here $x_n = Ry/(k_B T_K n^2)$ (k_B is the Boltzmann constant, n is the level to which the electron recombines, and $Ry = 13.6\,{\rm eV}$ is the Rydberg unit of energy) and $\bar{g}_{\rm ff} \approx 1.1$–$1.2$ and $g_{\rm fb}(n) \approx 1.05$–$1.09$ are the thermally averaged Gaunt factors for free–free and free–bound emission (Karzas & Latter 1961, values from). The initial level n' is determined by the emitted photon frequency and satisfies the condition $cR_\infty/n'^2 < \nu < cR_\infty/(n'-1)^2$, where $R_\infty = 1.1 \times 10^7\ {\rm m^{-1}}$ is the Rydberg constant.

The continuum luminosity per frequency interval (L_ν) is related to the Lyα luminosity emitted from the galaxies by $L_{\rm cont} = L_\nu \times d\nu(4\,{\rm Å}) = f_{{\rm Ly}\alpha} Q_{{\rm Ly}\alpha} E_{{\rm Ly}\alpha}{\rm SFR}(M, z)$, where $Q_{{\rm Ly}\alpha}$ is the number of emitted Lyα photons per solar mass in star formation. We then obtain $Q_{{\rm Ly}\alpha}^{\rm free-free} = 2.13 \times 10^{53}\ M_\odot^{-1}$ for free–free emission and $Q_{{\rm Ly}\alpha}^{\rm free-bound} = 2.22 \times 10^{55}\ M_\odot^{-1}$ for free–bound emission.

During recombination there is also the probability of two-photon emission and although these photons have frequencies below the Lyα frequency there is a small fraction of them of $Q_{{\rm Ly}\alpha}^{\rm 2-photon}$ that are emitted so close to the Lyα line, which are included in the Lyα intrinsic width.

The number of Lyα photons that can be originated due to two-photon emission during recombination is given by

$$Q_{{\rm Ly}\alpha}^{\rm 2-photon} = \int_{\nu_{{\rm Ly}\alpha+2\,{\rm Å}}}^{\nu_{{\rm Ly}\alpha}} \frac{2}{\nu_{{\rm Ly}\alpha}} P(\nu/\nu_{{\rm Ly}\alpha}) d\nu, \quad (18)$$

where $P(y)dy$ is the normalized probability that in a two-photon decay one of them is the range $dy = d\nu/\nu_{{\rm Ly}\alpha}$ and $1 - f_{{\rm Ly}\alpha} \approx 1/3$ is the probability of two-photon emission during a hydrogen $n = 2 \rightarrow 1$ transition. The probability of two-photon decay was fitted by Fernandez & Komatsu (2006) using Table 4 of Brown & Mathews (1970) as

$$P(y) = 1.307\text{–}2.627(y - 0.5)^2 + 2.563(y - 0.5)^4 - 51.69(y - 0.5)^6. \quad (19)$$

Finally, the different contributions to the total Lyα luminosity from galaxies due to continuum emission, $L_{\rm cont}^{\rm GAL} = L_{\rm cont}^{\rm stellar} + L_{\rm cont}^{\rm free-free} + L_{\rm cont}^{\rm free-bound} + L_{\rm cont}^{\rm 2-photon}$, are given by

$$L_{\rm cont}^{\rm stellar}(M, z) = f_{{\rm Ly}\alpha} Q_{{\rm Ly}\alpha}^{\rm stellar} E_{{\rm Ly}\alpha}{\rm SFR}(M, z) \approx 5.12 \times 10^{40} f_{{\rm Ly}\alpha} \frac{{\rm SFR}(M, z)}{M_\odot\ {\rm yr^{-1}}}\ {\rm erg\ s^{-1}} \quad (20)$$

for stellar emission,

$$L_{\rm cont}^{\rm free-free}(M, z) = f_{{\rm Ly}\alpha} Q_{{\rm Ly}\alpha}^{\rm stellar} E_{{\rm Ly}\alpha}{\rm SFR}(M, z) \approx 1.10 \times 10^{35} f_{{\rm Ly}\alpha} \frac{{\rm SFR}(M, z)}{M_\odot\ {\rm yr^{-1}}}\ {\rm erg\ s^{-1}} \quad (21)$$

for free–free emission,

$$L_{\rm cont}^{\rm free-bound}(M, z) = f_{{\rm Ly}\alpha} Q_{{\rm Ly}\alpha}^{\rm stellar} E_{{\rm Ly}\alpha}{\rm SFR}(M, z) \approx 1.47 \times 10^{37} f_{{\rm Ly}\alpha} \frac{{\rm SFR}(M, z)}{M_\odot\ {\rm yr^{-1}}}\ {\rm erg\ s^{-1}} \quad (22)$$

for free–bound emission, and

$$L_{\rm cont}^{\rm 2-photon}(M, z) = f_{{\rm Ly}\alpha} Q_{{\rm Ly}\alpha}^{\rm stellar} E_{{\rm Ly}\alpha}{\rm SFR}(M, z) \approx 2.41 \times 10^{38} f_{{\rm Ly}\alpha} \frac{{\rm SFR}(M, z)}{M_\odot\ {\rm yr^{-1}}}\ {\rm erg\ s^{-1}} \quad (23)$$

for two-photon emission.

Note that here we are only considering the part of the continuum emission from galaxies that could contribute to the same "Lyα redshift." There will be a continuum emission spectrum with frequencies below the Lyα line from the mechanisms above that will contribute to the same observation from lower redshifts and will generate a "foreground" to the Lyα signal that needs to be removed. This should be possible due to the smoothness of this background across frequency, in the same manner as foregrounds of the 21 cm signal are removed (e.g., Wang et al. 2006).

2.5. Modeling the Relation between Star Formation Rate and Halo Mass

Simulations of galaxy formation and observations indicate that the star formation of a halo increases strongly for small halo masses, but at high halo masses ($M \gtrsim 10^{11}\ M_\odot$) it becomes almost constant (Conroy & Wechsler 2009; Popesso et al. 2012).

In order to better estimate and constrain the SFR of a halo, we used three nonlinear SFR versus halo mass parameterizations that are in good agreement with different observational constraints. In *Sim1* we adjusted the SFR to reproduce a reasonable reionization history and an Lyα LF evolution compatible with different observational constraints, and in *Sim2* we adjusted the SFR versus halo mass relation to the parameterizations from the Guo et al. (2011) galaxy catalog (low halo masses) and the De Lucia & Blaizot (2007) galaxy catalog (high halo masses). *Sim2* results in an early reionization history with an optical depth to

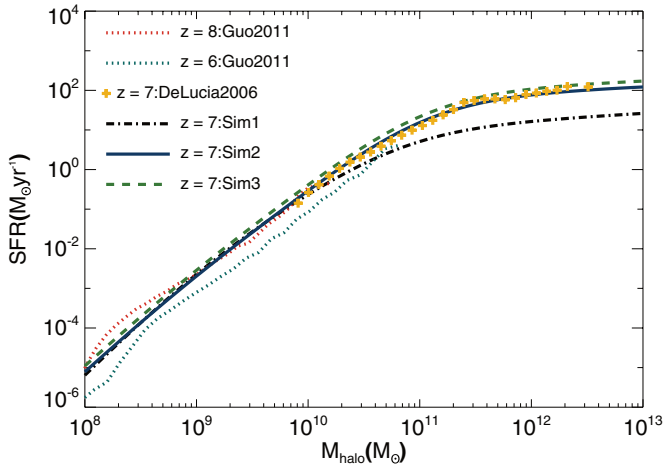

Figure 1. Star formation rate vs. halo mass. The dotted lines show the relations taken from the Guo et al. (2011) catalog for low halo masses at $z = 6$ (bottom dotted line) and $z = 8$ (upper dotted line); the yellow crosses show the relation taken from the DeLucia catalog for high halo masses at $z = 7$. The dash-dotted, solid, and dashed lines show the parameterizations used in simulations *Sim1*, *Sim2*, and *Sim3*, respectively, for $z = 7$.

(A color version of this figure is available in the online journal.)

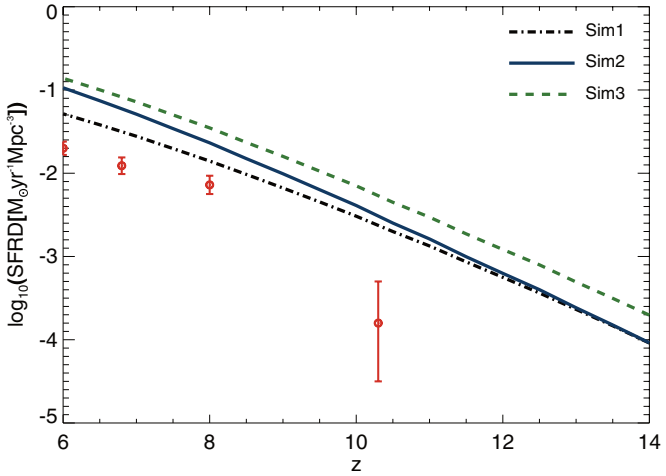

Figure 2. Star formation rate density evolution as a function of redshift. The blue solid line, the green dashed line, and the black dash-dotted line were obtained from simulations made using the SimFast21 code (for information about the code see Section 4 and Santos et al. 2010) and the SFR vs. halo mass relations from Equations (24)–(26). The red dots are observational constraints derived from the UV luminosities corrected for dust extinction from Bouwens et al. (2012b). Please note that these observational values correspond to high-mass galaxies, while our results integrate over the halo-mass function starting at $\sim 10^8$ solar masses (which at redshift 7 corresponds to star formation rates of $6.41 \times 10^{-5}\ M_\odot\ \mathrm{s}^{-1}$ for *Sim1*, $7.83 \times 10^{-6}\ M_\odot\ \mathrm{s}^{-1}$ for *Sim2*, and $1.1 \times 10^{-5}\ M_\odot\ \mathrm{s}^{-1}$ for *Sim3*), so our star formation rate densities are expected to be higher.

(A color version of this figure is available in the online journal.)

reionization compatible with the low bound of the current observational constraints. Finally, *Sim3* has the same halo mass dependence as *Sim2* but evolves with redshift in a similar way to the De Lucia & Blaizot (2007) and Guo et al. (2011) galaxy catalogs.

We parameterized the relations between the SFR and halo mass as

$$\frac{\mathrm{SFR}(M,z)}{M_\odot/\mathrm{yr}} = (2.8\times10^{-28})M^a\left(1+\frac{M}{c_1}\right)^b\left(1+\frac{M}{c_2}\right)^d, \quad (24)$$

where $a = 2.8$, $b = -0.94$, $d = -1.7$, $c_1 = 1\times10^9\ M_\odot$, and $c_2 = 7\times10^{10}\ M_\odot$ for *Sim1*;

$$\frac{\mathrm{SFR}(M,z)}{M_\odot/\mathrm{yr}} = 1.6\times10^{-26}M^a\left(1+\frac{M}{c_1}\right)^b \times\left(1+\frac{M}{c_2}\right)^d\left(1+\frac{M}{c_3}\right)^e, \quad (25)$$

where $a = 2.59$, $b = -0.62$, $d = 0.4$, $e = -2.25$, $c_1 = 8\times10^8\ M_\odot$, $c_2 = 7\times10^9\ M_\odot$, and $c_3 = 1\times10^{11}\ M_\odot$ for *Sim2*; and

$$\frac{\mathrm{SFR}(M,z)}{M_\odot/\mathrm{yr}} = 2.25\times10^{-26}\,(1+0.075\times(z-7))\,M^a \times\left(1+\frac{M}{c_1}\right)^b\left(1+\frac{M}{c_2}\right)^d\left(1+\frac{M}{c_3}\right)^e, \quad (26)$$

where $a = 2.59$, $b = -0.62$, $d = 0.4$, $e = -2.25$, $c_1 = 8\times10^8\ M_\odot$, $c_2 = 7\times10^9\ M_\odot$, and $c_3 = 1\times10^{11}\ M_\odot$ for *Sim3*. Figure 1 shows these relations.

In Figure 2, the strong decline in the observational SFR density (SFRD) from $z \approx 8$ to $z \approx 10$, imposed by the observational point at $z = 10.3$, was obtained with the observation of a single galaxy using the Hubble Deep Field 2009 two years' data (Bouwens et al. 2011; Oesch et al. 2012). It was argued in Bouwens et al. (2012a), based on an analytical calculation, that even with such low SFRD at high redshifts it was possible to obtain an optical depth to reionization compatible with the value obtained by *Wilkinson Microwave Anisotropy Probe* (*WMAP*; $\tau = 0.088 \pm 0.015$) (Komatsu et al. 2011). However, this derivation would imply a high escape fraction of ionizing radiation, and that reionization would end at $z \approx 8$, which is hard to reconcile with the constraints from observations of quasar spectra (Mesinger & Haiman 2007; Zaldarriaga et al. 2008). Our SFRDs are considerably higher than the current observational constraints, although the difference can be explained by a systematic underestimation of the SFR in observed galaxies. Moreover, current observations only probe the high-mass end of the high-redshift galaxies' mass function, which will underestimate the SFRD (also the obtained SFRs have very high error bars due to uncertainties in the correction due to dust extinction, the redshift, and the galaxy type). In the following sections the results shown were obtained using *Sim1* unless stated otherwise.

2.6. Total Lyα Luminosity: Comparison with Observations

In the previous sections we calculated the Lyα luminosity as a function of the SFR for several effects. The commonly used "empirical" relation between these two quantities is (Jiang et al. 2011)

$$L_{\mathrm{Gal}} = 1.1\times10^{42}\frac{\mathrm{SFR}(M,z)}{M_\odot\ \mathrm{yr}^{-1}}\ \mathrm{erg\ s}^{-1}, \quad (27)$$

and it is based on the relation between SFR and the Hα luminosity from Kennicutt (1998a) and on the line emission ratio of Lyα to Hα in case B recombinations calculated assuming a gas temperature of 10^4 K. This empirical relation gives the Lyα luminosity without dust absorption (we have labeled it *K98* for the remainder of the paper).

Our relation between luminosity and star formation is mass dependent (both from the escape fraction and due to the

Table 2
Average Luminosity per Star Formation Rate (in Units of erg $s^{-1}/M_\odot$ yr^{-1}) Averaged over the Halo Mass Function for Redshifts 10, 9, 8, and 7, from Top to Bottom

$A_{rec}(z)$	$A_{exc}(z)$	$A_{cool}(z)$	$A_{cont}(z)$	$A_{total}(z)$
4.4×10^{41}	1.1×10^{41}	1.3×10^{39}	8.1×10^{40}	6.4×10^{41}
1.2×10^{42}	3.2×10^{41}	7.8×10^{38}	6.4×10^{40}	1.6×10^{42}
9.3×10^{41}	2.4×10^{41}	4.9×10^{38}	4.9×10^{40}	1.2×10^{42}
8.5×10^{41}	2.2×10^{41}	3.3×10^{38}	3.6×10^{40}	1.1×10^{42}

expression from the cooling mechanism), so in order to compare it with the result above, we calculate

$$A(z) = \frac{\langle L_{\rm Gal}(M, z)\rangle}{\langle {\rm SFR}(M, z)\rangle}, \quad (28)$$

where the average $\langle x\rangle$ of quantity x is done over the halo mass function for the mass range considered. The results are presented in Table 2 for a few redshifts.

Although our Lyα luminosities per SFR are slightly higher, at least for low redshifts, we point out that the "empirical" relation is based on a theoretical calculation that only accounts for Lyα emission due to recombinations. Moreover, the observational measurements of Hα and Lyα are primarily made at low redshifts, where the absorption of Lyα photons by dust in galaxies is expected to be high. Our relation has the advantage of evolving with redshift since it accounts for the evolution of the escape fraction of ionizing photons and for the evolution of the escape fraction of Lyα photons. This z-dependence is not present in the standard empirical relation. This redshift evolution of the UV photons' escape fraction is a consequence of the increase in the number of massive galaxies with more clumpy structure as the redshift decreases. The star-forming regions of massive galaxies are embedded in clumps, and therefore it becomes more difficult for the ionizing photons to escape from such dense regions (Razoumov & Sommer-Larsen 2010; Yajima et al. 2011). The redshift evolution of the relation presented in Equation (28) justifies why a theoretical calibration between Lyα luminosity and the SFR of a galaxy is useful for our work.

To check the consistency between our theoretical estimation of the Lyα luminosity and the existing observations during reionization, we show in Figure 3 the LF using two of the SFR versus halo mass parameterizations presented in Section 2.5. This prediction is then compared to Lyα LFs of photometric identified objects in Shimasaku et al. (2006) and in Kashikawa et al. (2006) near the end of the reionization epoch.

Our LFs were calculated assuming a minimum halo mass of $8 \times 10^8\ M_\odot$, which corresponds to a minimum luminosity of 3.72×10^{36} erg s^{-1} for *Sim1*, 4.49×10^{36} erg s^{-1} for *Sim2*, and 6.22×10^{36} erg s^{-1} for *Sim3*. The agreement between our LFs and observations is reasonable for *Sim1*; however, our *Sim2* overpredicts the abundance of high-luminosity Lyα emitters. This difference can be due to sample variance or a result of the high sensitivity of theoretical predictions to several parameters in our model. We point out that the luminosity range relevant for this comparison falls in a halo mass range outside the one for which the escape fraction of UV radiation we are using was estimated, so we could easily get a better fit between observations and *Sim2* by reducing this escape fraction for high halo masses. This difference could also be related with the choice of halo mass function. Here we choose the Sheth–Tormen halo mass function (Sheth & Tormen 1999), which has been shown to fit low-redshift simulations more accurately, but it is yet to be established the extent to which such a halo mass function can reproduce the halo distribution during reionization. Another possible explanation for this difference is the existence of a small amount of neutral gas in the IGM, which would severely decrease the observed Lyα luminosity from galaxies. Also, we could have decreased the high-luminosity end of our LFs if we had use an Lyα escape fraction that decreased with halo mass such as the one used in Forero-Romero et al. (2011). We do not consider a model fit to the data to optimize various parameters in our model given that the current constraints on the observed Lyα LFs have large overall uncertainties, especially considering variations from one survey to another.

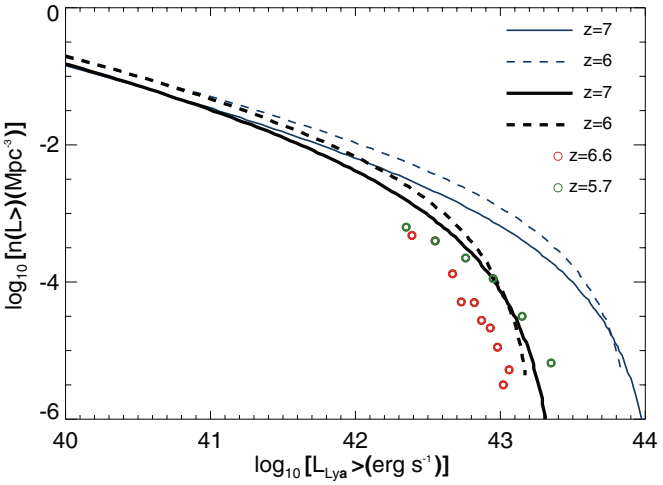

Figure 3. Lyα luminosity functions obtained with our calculations are shown for redshifts $z = 6$ (dashed lines) and $z = 7$ (solid lines) for *Sim1* (black thick lines) and *Sim2* (blue thin lines). The green and red circles show the intrinsic (i.e., not affected by the IGM) Lyα LF from photometric identified objects in Shimasaku et al. (2006) and in Kashikawa et al. (2006) for $z = 5.7$ and 6.6, respectively.

(A color version of this figure is available in the online journal.)

2.7. Lyα Average Intensity

In this section and the next one we will attempt to estimate the intensity and power spectrum of the Lyα signal using an analytical model. In Section 4, we will improve the estimation by doing the same calculation using a semi-numerical simulation.

The total intensity of Lyα emission can be obtained from the combined luminosity of Lyα photons associated with different mechanisms described in the previous sub-sections, such that

$$\bar{I}_{\rm Gal}(z) = \int_{M_{\rm min}}^{M_{\rm max}} dM \frac{dn}{dM} \frac{L_{\rm Gal}(M, z)}{4\pi D_{\rm L}^2} y(z) D_{\rm A}^2, \quad (29)$$

where dn/dM is the halo mass function (Sheth & Tormen 1999), M is the halo mass, $M_{\rm max} = 10^{13}\ M_\odot$, $M_{\rm min} = M_{\rm OB}$, $D_{\rm L}$ is the proper luminosity distance, and $D_{\rm A}$ is the comoving angular diameter distance. Finally, $y(z) = d\chi/d\nu = \lambda_{{\rm Ly}\alpha}(1+z)^2/H(z)$, where χ is the comoving distance, ν is the observed frequency, and $\lambda_{{\rm Ly}\alpha} = 2.46 \times 10^{-15}$ m is the rest-frame wavelength of the Lyα line.

The evolution of the Lyα intensity predicted by this calculation is shown in Figure 4 together with the scaling expected under the "empirical" relation from Kennicutt (1998a) combined with an assumption related to the gas temperature. The intensities of Lyα emission from different sources are presented in Table 3 for several redshifts.

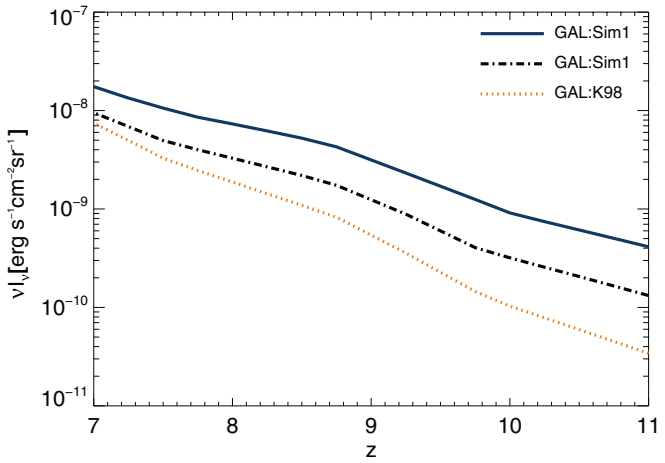

Figure 4. Lyα intensity from galaxies in erg s^{-1} cm^{-2} sr^{-1} as a function of redshift. The black dash-dotted line and the blue solid line were obtained using our theoretical calculation of the Lyα luminosity and the SFR halo mass relation from *Sim1* and *Sim2*, respectively. The orange dotted line uses the Lyα luminosity SFR relation based on the relation between SFR and the Hα luminosity from Kennicutt (1998a) and the line emission ratio of Lyα to Hα in case B recombinations calculated assuming a gas temperature of 10,000 K (labeled as the K98 relation). The K98 line is not corrected for dust absorption.

(A color version of this figure is available in the online journal.)

Table 3
Surface Brightness (in Observed Frequency times Intensity) of Lyα Emission from the Different Sources in Galaxies at $z \approx 7$, $z \approx 8$, and $z \approx 10$ for *Sim1*

Source of emission in (erg s^{-1} cm^{-2} sr^{-1})	$\nu I_\nu(z=7)$	$\nu I_\nu(z=8)$	$\nu I_\nu(z=10)$
Recombinations	7.3×10^{-9}	2.5×10^{-9}	2.3×10^{-10}
Excitations	1.9×10^{-9}	6.5×10^{-10}	6.0×10^{-11}
Cooling	2.8×10^{-12}	1.5×10^{-12}	4.7×10^{-13}
Continuum	3.1×10^{-10}	3.5×10^{-10}	3.0×10^{-11}
Total	9.5×10^{-9}	3.5×10^{-9}	3.2×10^{-10}

These intensities can be extrapolated to other SFRDs, assuming that the only change is in the amplitude of the SFR halo mass relations presented in Figure 1 by using the coefficients in Table 4.

The intensities from emission at $z \approx 7$, 8, and 10 are 9.5×10^{-9}, 3.5×10^{-9}, and 3.2×10^{-10} erg s^{-1} cm^{-2} sr^{-1}, respectively. Such an intensity is substantially smaller than the background intensity of integrated emission from all galaxies (around 1×10^{-5} erg s^{-1} cm^{-2} sr^{-1}; Madau & Pozzetti 2000), or from the total emission of galaxies during reionization, estimated to be at most 1×10^{-6} erg s^{-1} cm^{-2} sr^{-1} (Cooray et al. 2012).

2.8. Lyα Intensity Power Spectrum

The Lyα emission from galaxies will naturally trace the underlying cosmic matter density field, so we can write the Lyα line intensity fluctuations due to galaxy clustering as

$$\delta I_{\rm GAL} = b_{\rm Ly\alpha} \bar{I}_{\rm GAL} \delta(\mathbf{x}), \tag{30}$$

where $\bar{I}_{\rm GAL}$ is the mean intensity of the Lyα emission line, $\delta(\mathbf{x})$ is the matter overdensity at the location $\mathbf{x}$, and $b_{\rm Ly\alpha}$ is the average galaxy bias weighted by the Lyα luminosity (see, e.g., Gong et al. 2011).

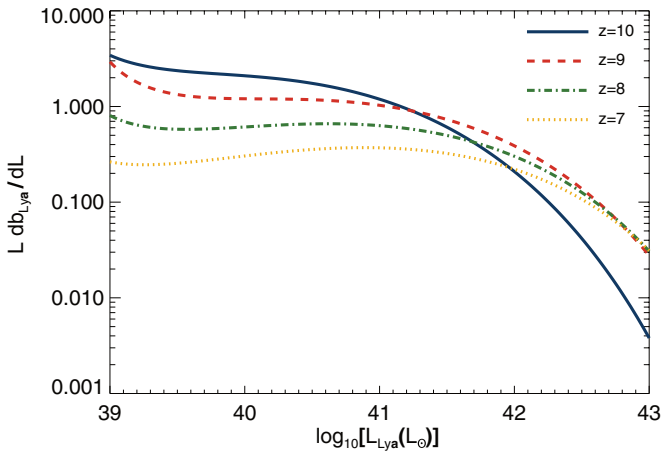

Figure 5. Bias between dark matter fluctuations and Lyα surface brightness (νI) from galaxies as a function of the galaxy Lyα luminosity at redshifts 7, 8, 9, and 10.

(A color version of this figure is available in the online journal.)

Table 4
Average Lyα Intensity from Galaxies per SFRD ($A_{\rm SFRD}$) in Units of erg s^{-1} cm^{-2} sr^{-1}/$M_\odot$ yr^{-1}, Calculated Using the Star Formation Rate Halo Mass Relation from Simulations *Sim1* and *Sim2*

Redshift	$A_{\rm SFRD}$(*Sim1*)	$A_{\rm SFRD}$(*Sim2*)
10	1.05×10^{-03}	2.20×10^{-03}
9	2.17×10^{-03}	3.75×10^{-03}
8	2.34×10^{-03}	3.15×10^{-03}
7	3.42×10^{-03}	3.42×10^{-03}

Using one of the relations between the SFR and halo mass from Section 2.5, we can calculate the luminosity and obtain the Lyα bias following Visbal & Loeb (2010):

$$b_{\rm Ly\alpha}(z) = \frac{\int_{M_{\rm min}}^{M_{\rm max}} dM \frac{dn}{dM} L_{\rm GAL}\, b(z, M)}{\int_{M_{\rm min}}^{M_{\rm max}} dM \frac{dn}{dM} L_{\rm GAL}}, \tag{31}$$

where $b(z, M)$ is the halo bias and dn/dM is the halo mass function (Sheth & Tormen 1999). We take $M_{\rm min} = 10^8\, M_\odot/h$ and $M_{\rm max} = 10^{13}\, M_\odot/h$. The bias between dark matter fluctuation and the Lyα luminosity, as can be seen in Figure 5, is dominated by the galaxies with low Lyα luminosity independently of the redshift.

We can then obtain the clustering power spectrum of Lyα emission as

$$P^{\rm clus}_{\rm GAL}(z, k) = b^2_{\rm Ly\alpha} \bar{I}^2_{\rm GAL} P_{\delta\delta}(z, k), \tag{32}$$

where $P_{\delta\delta}(z, k)$ is the matter power spectrum. The shot-noise power spectrum, due to discretization of the galaxies, is also considered here. It can be written as (Gong et al. 2011)

$$P^{\rm shot}_{\rm Ly\alpha}(z) = \int_{\rm M_{max}}^{\rm M_{min}} dM \frac{dn}{dM} \left(\frac{L_{\rm GAL}}{4\pi D_{\rm L}^2} y(z) D_{\rm A}^2 \right)^2. \tag{33}$$

The resulting power spectrum of Lyα emission from galaxies is presented in Figure 6. At all scales presented the Lyα intensity and fluctuations are dominated by the recombination emission from galaxies.

3. Lyα EMISSION FROM THE IGM

The Lyα emission from the IGM is mostly originated in recombinations and collisions powered by the ionizing

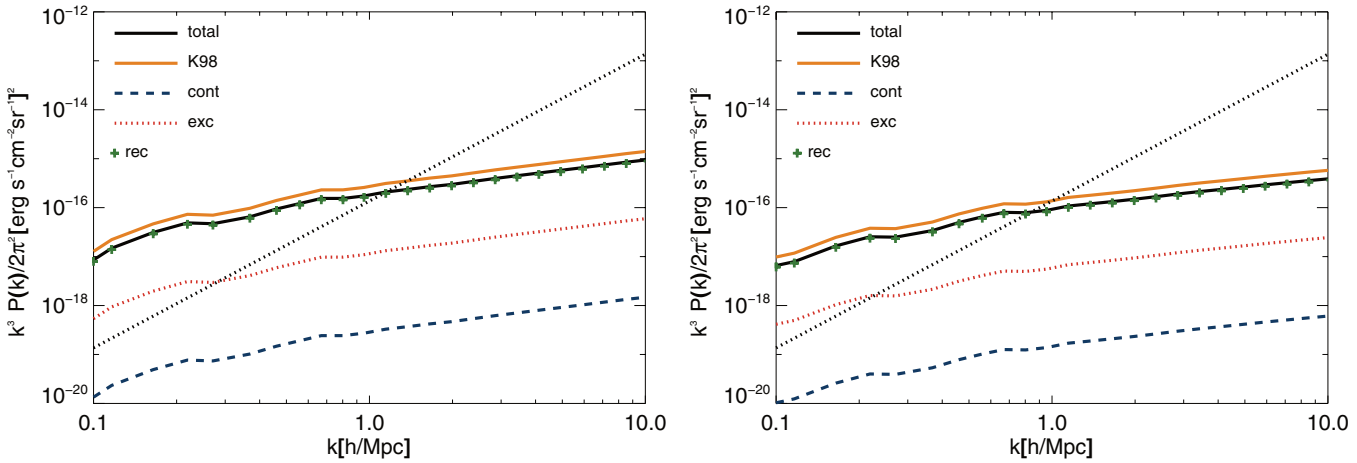

Figure 6. Clustering power spectrum of the Lyα surface brightness (νI) from galaxies at redshifts 7–10 (from top to bottom), from several sources: collisions and excitations, recombinations, and continuum emission with frequencies inside the Lyα width. The power spectra from cooling emission are not shown since they are several orders of magnitude smaller than the contributions from the other sources. Also shown are the total power spectra (clustering (solid black line) and shot-noise power spectra (dotted black line)) of the total contribution for Lyα emission in galaxies predicted by our theoretical calculation and total Lyα clustering power spectra predicted using the $K98$ relation (orange solid line).

(A color version of this figure is available in the online journal.)

background. These processes are similar to the ones described inside the galaxies, although, since the physical conditions of the gas in the IGM are different from those in the ISM, the intensity of Lyα emission can no longer be connected to the ionizing photon intensity using the previous relations. The biggest challenge in doing these calculations is to connect the IGM ionizations and heating of the gas to the emission of ionizing radiation and the SFR assumed in the previous sections. Moreover, in the IGM, we also have to take into account the contribution of continuum radiation from stars between the Lyα and the Lyman limit, which redshifts into the Lyα line.

In a schematic view, we have to take into account the following processes:

1. The amount of energy in UV photons that escapes the galaxy.
2. This energy will then be distributed in the IGM into
   (a) ionizations,
   (b) direct excitations (followed by emission, partially into the Lyα line), and
   (c) heating of the gas.
3. Taking into account the state of the IGM in terms of temperature and ionization, we can then further determine how much it will radiate through the Lyα line from
   (a) recombinations and
   (b) radiative cooling (usually through excitations followed by decay in several lines including Lyα).
4. The amount of Lyn photons that escape the galaxy, re-scattering in the IGM into Lyα photons.

The proper calculation of all these processes will require simulations, which we will address in Section 4. In the following sub-sections we review the contributions through analytical calculations in order to get a better understanding of the dominating effects.

3.1. Lyα Emission from Hydrogen Recombinations

The UV radiation that escapes the ISM into the IGM ionizes low-density clouds of neutral gas. Part of the gas in these clouds then recombines, giving rise to Lyα emission. The radiation emitted in the IGM is often referred to as fluorescence (Santos 2004). The comoving number density of recombinations per second in a given region, $\dot{n}_{\rm rec}$, is given by

$$\dot{n}_{\rm rec}(z) = \alpha n_e(z) n_{\rm H\,II}(z), \quad (34)$$

where α changes between the case A and the case B recombination coefficient and $n_{\rm H\,II} = x_i(n_b(1 - Y_p)/((1–3)/4Y_p))$ is the ionized hydrogen comoving number density (x_i is the ionization fraction, n_b the baryonic comoving number density). The free electron density can be approximated by $n_e = x_i n_b$.

The recombination coefficients are a function of the IGM temperature, T_K. The case A comoving recombination coefficient is appropriate for the highly ionized low-redshift universe (Furlanetto et al. 2006),

$$\alpha_A \approx 4.2 \times 10^{-13} (T_K/10^4\ {\rm K})^{-0.7} (1+z)^3\ {\rm cm^3\ s^{-1}}, \quad (35)$$

while the case B comoving recombination coefficient is appropriate for the high-redshift universe,

$$\alpha_B \approx 2.6 \times 10^{-13} (T_K/10^4\ {\rm K})^{-0.7} (1+z)^3\ {\rm cm^3\ s^{-1}}. \quad (36)$$

The use of a larger recombination coefficient when the process of hydrogen recombination is close to its end accounts for the fact that, at this time, ionizations (and hence recombinations) take place in dense, partially neutral gas (Lyman-limit systems) and the photons produced after recombinations are consumed inside these systems, so they do not help ionize the IGM (see, e.g., Furlanetto et al. 2006).

The fraction of Lyα photons emitted per hydrogen recombination, $f_{\rm rec}$, is temperature dependent, so we used the parameterization for $f_{\rm rec}$ made by Cantalupo et al. (2008) using a combination of fits tabulated by Pengelly (1964) and Martin (1988) for $T_K > 10^3$ and $T_K < 10^3$, respectively:

$$f_{\rm rec} = 0.686\text{–}0.106 \log_{10}(T_K/10^4\ {\rm K}) - 0.009 (T_K/10^4\ {\rm K})^{-0.4}. \quad (37)$$

The luminosity density (per comoving volume) in Lyα from hydrogen recombinations in the IGM, $\ell_{\rm rec}^{\rm IGM}$, is then given by

$$\ell_{\rm rec}^{\rm IGM}(z) = f_{\rm rec} \dot{n}_{\rm rec} E_{{\rm Ly}\alpha}. \quad (38)$$

3.2. Lyα Emission from Excitations in the IGM

The UV radiation that escapes the galaxies without producing ionization ends up ionizing and exciting the neutral hydrogen in the IGM and heating the gas around the galaxies. The high energetic electron released after the first ionization spends its energy in collisions/excitations, ionizations, and heating the IGM gas until it thermalizes (Shull & van Steenberg 1985). We estimated the contribution of the direct collisions/excitations to the Lyα photon budget and concluded that it is negligible.

The Lyα luminosity density due to the collisional emission (radiative cooling in the IGM), $\ell_{\rm exc}^{\rm IGM}$, is given by

$$\ell_{\rm exc}^{\rm IGM}(z) = n_e n_{\rm H\,I} q_{\rm Ly\alpha} E_{\rm Ly\alpha}, \quad (39)$$

where $n_{\rm H\,I} = n_b(1 - x_i)((1 - Y_p)/((1–3)/4Y_p))$ is the neutral hydrogen density, x_i is the IGM ionized fraction, and $q_{\rm Ly\alpha}$ is the effective collisional excitation coefficient for Lyα emission, which we calculated in the same way as Cantalupo et al. (2008), but using different values for the gas temperature and IGM ionization fraction.

Considering excitation processes up to the level $n = 3$ that could eventually produce Lyα emission, the effective collisional excitation coefficient is given by

$$q_{\rm Ly\alpha} = q_{1,2p} + q_{1,2s} + q_{1,3p}. \quad (40)$$

The collisional excitation coefficient for the transition from the ground level (1) to the level (nl) is given by

$$q_{1,nl} = \frac{8.629 \times 10^{-6}}{T_K^{1/2}} \frac{\Omega(1, nl)}{\omega_1} e^{E_{1,n}/k_B T_K} \ {\rm cm^3\ s^{-1}}, \quad (41)$$

where $\Omega(1, nl)$ is the temperature-dependent effective collision strength, ω_1 is the statistical weight of the ground state, $E_{1,n}$ is the energy difference between the ground and the nl level, and k_B is the Boltzmann constant.

3.3. Scattering of Lyn Photons Emitted from Galaxies

Continuum emission of photons, by stars, from Lyα to the Lyman limit travels until it reaches one of the Lyn lines, where it gets scattered by neutral hydrogen. Most of this scattering will have as an end result the production of Lyα photons, which eventually redshift out of the line. Since a considerable fraction of these photons only reach a given Lyn frequency in the IGM, this Lyα emission is formed as a flux that decays with r^2 around the star that emitted the continuum photons, so it appears diluted in frequency in line observations of point sources (Chen & Miralda-Escudé 2008). These continuum photons are much less likely to be absorbed by the dust in the ISM than photons originated in recombinations.

In intensity mapping, the frequency band observed is much larger than in line observations, so in principle all the continuum Lyα photons can be detected. Using the spectral energy distribution (SED) made with the code from Maraston (2005), we estimated that the number of photons emitted by stars between the Lyα plus the Lyα equivalent width and the Lyman limit is equivalent to $Q_{\rm Lyn}^{\rm IGM} = 9.31 \times 10^{60}\, M_\odot^{-1}\ {\rm s^{-1}}$. The higher frequency photons are absorbed by hydrogen atoms as they reach the Lyβ frequency, re-emitted, and suffer multiple scattering until they reach the Lyα line. The fraction of the continuum photons emitted close to the Lyα line have already redshifted to lower frequencies before reaching the IGM, so they will not be scattered by the neutral hydrogen in the IGM and will not contribute to the radiative coupling of the 21 cm signal (they are already included in the calculation of the Lyα emission from galaxies).

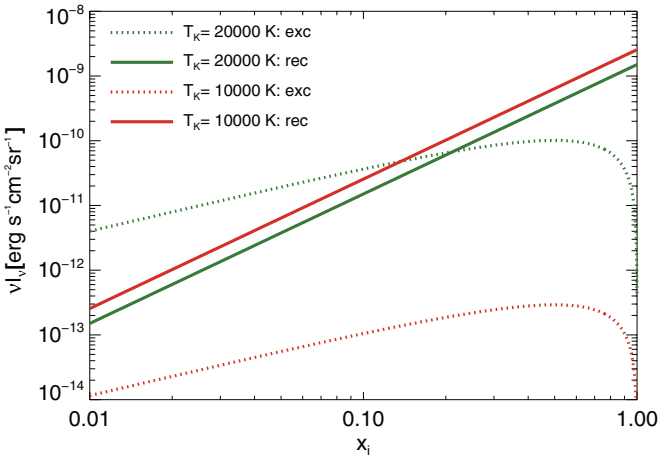

Figure 7. Intensity of Lyα emission at redshift 7 due to recombinations and excitations in the IGM as a function of the hydrogen ionized fraction. The green and red lines assume a constant gas temperature of 20,000 K and 10,000 K, respectively.

(A color version of this figure is available in the online journal.)

The intensity of this emission was calculated with a stellar emissivity that evolves with frequency as $\nu^{-\alpha}$ with $\alpha = 0.86$ and normalized to $Q_{\rm Lyn}^{\rm IGM}$. The Lyα luminosity density originated from continuum stellar radiation and emitted in the IGM, $\ell_{\rm cont}^{\rm IGM}$, is then approximately given by

$$\ell_{\rm cont}^{\rm IGM}(z) \approx Q_{\rm ly\alpha}^{\rm IGM} E_{\rm Ly\alpha} {\rm SFRD}(z), \quad (42)$$

where the SFRD is in units of $M_\odot\ {\rm s^{-1}}$. Note that in Section 4, this calculation is done through a full simulation.

3.4. Lyα Intensity

We calculated the intensities for the several Lyα sources in the IGM from their luminosity densities using

$$\bar{I}_{\rm IGM}(z) = \frac{\ell^{\rm IGM}(z)}{4\pi D_L^2} y(z) D_A^2. \quad (43)$$

The luminosity and hence the intensity of Lyα emission in the IGM depend on local values of the hydrogen ionized fraction, the gas temperature, and the gas density. These parameters are correlated with each other, and so theoretical calculations of the average intensity made with the average of these parameters may be misleading. Since this emission is dominated by overdense regions, a clumping factor of a few units is usually assumed in theoretical calculations. However, we decided to estimate this intensity without using a clumping factor since its effect can be extrapolated from the intensity without clumping. The intensity of Lyα emission due to recombinations or collisions in the IGM is shown in Figure 7 as a function of the hydrogen ionized fraction for different values of the gas temperature.

Even for a fixed average IGM ionized fraction, the intensity of Lyα emission is the result of emission from several regions, and so all the values shown in Figure 7 are relevant. As can be seen in Figure 7, the intensity of Lyα due to recombinations and collisions in the IGM is very sensitive to the gas temperature and to the fluctuations in the IGM ionized fraction.

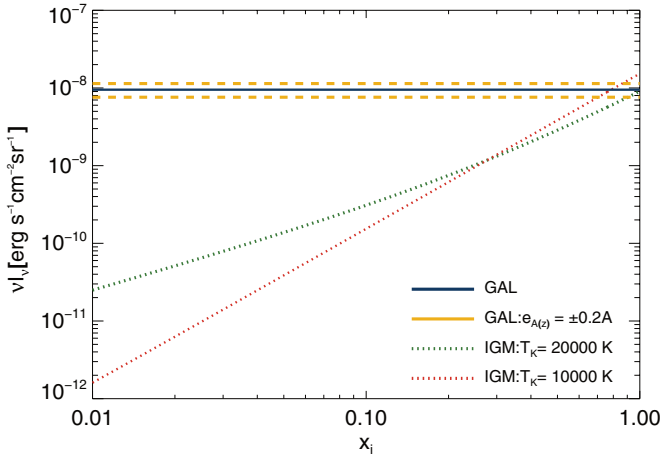

Figure 8. Intensity of Lyα emission at redshift 7 from the IGM and from galaxies as a function of the hydrogen ionized fraction and including all contributions. The green and red lines are the intensity of Lyα emission in the IGM assuming a constant gas temperature of 20,000 K and 10,000 K, respectively. The blue solid line is the intensity of Lyα emission from galaxies as calculated in the previous section. The yellow dashed lines show the intensity in galaxies assuming an error in $A(z)$ of 20% due to the uncertainty in the ionizing photons' escape fraction and due to the uncertainty in the emissivity of ionizing photons. The intensities in the IGM were calculated assuming a clumping factor of 6 compatible with current conservative estimates (Pawlik et al. 2010).

(A color version of this figure is available in the online journal.)

Numerical simulations predict that the temperatures in the hydrogen gas in the IGM can vary from 5000 to 20,000 K (Davé et al. 2001; Smith et al. 2011). The theoretical intensities of Lyα emission in galaxies and in the IGM shown in Figure 8 indicate that unless the IGM clumping factor is very high, or the Lyα photon escape fraction is very low, the Lyα intensity from the IGM at $z = 7$ is lower than the emission from galaxies. At higher redshifts the SFRD will decrease, causing the Lyα intensities from galaxies and from the IGM to decrease. The escape fraction of UV photons from galaxies increases as the redshift increases, which will contribute negatively to the intensity of emission in galaxies and positively to the intensity of emission in the IGM. At high redshifts the IGM ionized fraction is small, which contributes to a strong decrease in the intensity of emission from the IGM compared to the intensity at $z = 7$.

4. Lyα INTENSITY AND POWER SPECTRUM USING NUMERICAL SIMULATIONS

The intensity of Lyα emission in the IGM at a given time and a given region is proportional to the ionized fraction, the gas temperature, and the matter density in that region. Since these three quantities are correlated, the use of average values in the Lyα intensity calculation highly underestimates the emission in the more overdense regions. Also the evolution of the average of the IGM ionized fraction is poorly known during the EoR.

Some of these problems can be resolved using a computational code able to produce simulations of the IGM ionized fraction, the gas temperature, and the matter density in a volume high enough to properly represent our universe. The use of simulations has an additional advantage of allowing the calculation of the three-dimensional power spectra of Lyα emission in the IGM without the need for assuming a bias relation with the underlying dark matter distribution.

In this section we will estimate the inhomogeneous Lyα intensity from galaxies and the IGM using a modified version of the SimFast21 code (Santos et al. 2010). Given a set of astrophysical and cosmological parameters, this code is able to consistently produce three-dimensional simulations of the dark matter density field, the ionization field, the SFRD, the scattering of Lyn photons in the IGM, the X-ray heating of the IGM, and even 21 cm spin and brightness temperature fluctuations for the several redshifts of the EoR.

A proper calculation of all the heating and cooling mechanisms would add a high level of complexity to this calculation and would require a small redshift step in the IGM fraction calculation, so we assumed a constant temperature in ionized regions of 10,000 K. Moreover, the results from our calculations can be easily extrapolated to account for a higher temperature. For example, for a temperature of 20,000 K the number of recombinations in the IGM would decrease by a factor of 1.7 and the number of collisions would increase more than two orders in magnitude. Assuming that the clumping of the IGM is not very high, and so Lyα recombination emission dominates over collisional emission during most of the EoR, this higher temperature would cause a small decrease in the intensity of emission in the IGM and the reionization period would be less extended than what we predict in Section 4.1. We made a few modifications to the SimFast21 code in order to provide a consistent description of the ionization history and its relations to the Lyα emission, which we now describe.

4.1. IGM Ionized Fraction Calculation

In the previous version of the SimFast21 code, the IGM ionized fraction was computed assuming that at each redshift the ionization state of a region could be estimated from the collapsed mass in that region assuming a linear relation between collapsed mass and ionizing power. So a given spherical region of radius R is considered ionized if (Furlanetto et al. 2006)

$$\zeta M_{\rm coll}(R) \geqslant M_{\rm tot}(R), \tag{44}$$

where $M_{\rm coll}$ is the collapsed mass that corresponds to the total mass in halos in that region, $M_{\rm tot}$ is the total mass in the region, and ζ is an ionizing efficiency parameter. This efficiency parameter tries to include all the ionizations and recombinations produced by a halo as a function of its mass but has no actual physical meaning, although its use is somewhat justified by the large uncertainty in the astrophysical quantities involved in the determination of the relation between halo mass and ionizing efficiency and in the adjustment of this parameter in order to reproduce a reionization history compatible with observations.

In order to calculate the Lyα field, however, we need to include the recombinations in the IGM explicitly, as well as directly relate the ionization process to the emitted stellar radiation. We therefore modified the SimFast21 code to include these improvements. This new method allows a nonlinear relation between collapsed mass and ionizing power, and all the parameters involved in the calculation have values based on current astrophysical constraints. Also, the size of ionized regions is now set by the volume at which the total ionizing emissivity of the sources it contains equals the number of recombinations so that the system is in equilibrium. For each redshift the implementation of this method was done with the following steps:

1. A halo catalog with the mass and three-dimensional spatial positions was generated using the same method used in the original version of the SimFast21 code.
2. We calculated SFRs from the halo catalogs using the nonlinear relations in Equations (24)–(26).

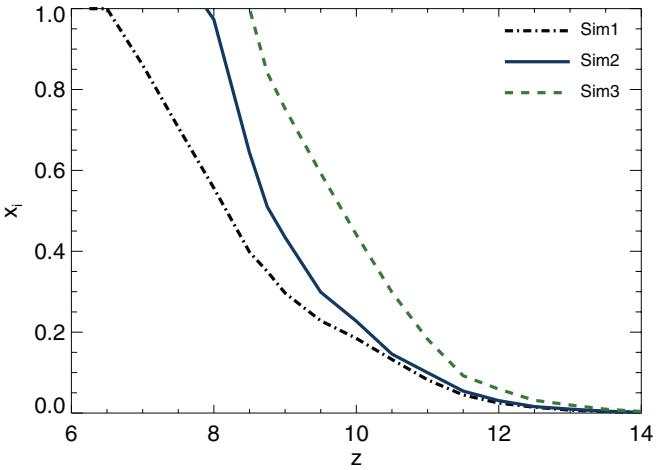

Figure 9. Evolution of the IGM ionized fraction as a function of redshift for the three star formation rate halo mass parameterizations shown in Section 2.5.
(A color version of this figure is available in the online journal.)

3. We used Equation (4) to obtain the halo ionizing rate, $\dot{N}_{\rm ion}$, and we corrected for the presence of helium using $A_{\rm He}$ and multiplied it by $f_{\rm esc}$, to account for the photons consumed inside the galaxies:

$$\dot{N}_{\rm ion}^{\rm IGM}(z, M) = A_{\rm He}\dot{N}_{\rm ion}(M) f_{\rm esc}(z, M). \quad (45)$$

   The UV ionizing rates of the halos, $\dot{N}_{\rm ion}^{\rm IGM}$, were then put in three-dimensional boxes.
4. Three-dimensional boxes with the rate of recombinations in each cell, $\dot{N}_{\rm rec}^{\rm IGM} = V_{\rm cell} \times \dot{n}_{\rm rec}^{\rm IGM}$, were obtained from a dark matter density simulation made with the SimFast21 code using Equation (34) with x_i set to 1 and $T_K = 10^4$ K.
5. Following the same procedure as in the original version of the SimFast21 code, we applied a series of top-hat filters of decreasing size (this filtering procedure was done in Fourier space) to the ionizing rate and the recombination rate boxes in order to calculate the region ionizing rate and recombination rate.
6. At each filtering step of radius R we found the ionized regions (H II bubbles) by checking if the region ionizing rate was equal to or higher than its recombination rate. With this method H II bubbles are always fully ionized:

$$\dot{N}_{\rm ion}^{\rm IGM}(z, R) \geqslant \dot{N}_{\rm rec}^{\rm IGM}. \quad (46)$$

4.2. Intensity from Recombinations and Collisions in the IGM

The SimFast21 code was built to calculate the IGM ionized state assuming two types of regions: one fully ionized (inside the H II bubbles) and the other fully neutral. The intensity of Lyα emission in the IGM due to recombinations is a smooth function of the IGM ionized fraction and is dominated by emission from fully ionized regions (see Figure 7), so the output of the SimFast21 code is good enough to estimate this intensity.

Collisions between electrons and neutral hydrogen atoms can also lead to Lyα emission; however, as was explained in Section 3.2, collisional Lyα emission only occurs in partly ionized regions, mainly in the edge of H II bubbles, so the estimation of this emission requires a more detailed description of the IGM ionized state than the one given by the limited resolution of semi-numerical simulations. Collisions are most important in regions where the IGM ionized fraction is locally close to 0.5 and the temperatures are high. Since high-temperature regions are likely to be highly ionized, we can deduce with the help of Figure 7 that Lyα emission from recombinations is dominant over Lyα emission from collisions in the IGM.

Table 5
Surface Brightness (in Observed Frequency times Intensity) of Lyα Emission from the Different Sources in the IGM at $z \approx 7$, $z \approx 8$, and $z \approx 10$

Source of emission in (erg s^{-1} cm^{-2} sr^{-1})	$\nu I_\nu(z = 7)$	$\nu I_\nu(z = 8)$	$\nu I_\nu(z = 10)$
Recombinations	9.3×10^{-10}	4.8×10^{-10}	9.6×10^{-11}
Continuum	3.5×10^{-13}	1.2×10^{-13}	1.5×10^{-14}
Total	1.6×10^{-9}	6.7×10^{-10}	1.1×10^{-10}

4.3. Intensity from the Scattering of Lyn Photons in the IGM

The IGM Lyα intensity from scattering of Lyn photons emitted from galaxies can also be calculated using data from the code SimFast21. This code uses Equation (10) in Santos et al. (2010) to calculate the spherical average of the number of Lyα photons, J_α, hitting a gas element per unit proper area per unit time per unit frequency per steradian. The Lyα intensity originated from these continuum photons is given by

$$I_{\rm cont}^{\rm IGM} = \frac{6 J_\alpha E_{\rm Ly\alpha} D_{\rm A}^2}{(1+z)^2 D_{\rm L}^2}. \quad (47)$$

4.4. Results

Using the prescriptions described in the previous sections, we ran simulations *Sim1*, *Sim2*, and *Sim3* with a volume of 54^3 h^{-3} Mpc^3 and 1800 cells from redshift 14 to redshift 6. The obtained IGM ionization fractions, at redshift 7, where $x_i = 0.86$ for simulation *Sim1* and $x_i = 1.0$ for simulations *Sim2* and *Sim3*. These values are consistent with the current most likely values for this parameter, $0.8 \leqslant x_i(z = 7) \leqslant 1.0$ (Mitra et al. 2012). The IGM ionized fraction evolution for *Sim2* and for *Sim3* (see Figure 9) resulted in optical depths to reionization of 0.073 and 0.082. These optical depths are consistent with the value obtained by *WMAP* ($\tau = 0.088 \pm 0.015$; Komatsu et al. 2011). The optical depth corresponding to *Sim1* is 0.66, which is lower than the current observational constraints. Based on the optical depth constraint, *Sim2* and *Sim3* have the most likely reionization histories, and the IGM ionized fraction evolution obtained with *Sim1* can be seen as a lower bound.

The intensities of Lyα emission from galaxies at redshift 7 obtained with the SimFast21 code are similar to the more theoretical estimates summarized in Table 3.

Intensities of Lyα emission in the IGM made with the same code are presented in Table 5.

The intensity values found in Tables 3 and 5 and the theoretical estimations plotted in Figure 8 indicate that for the Lyα intensity from the IGM to reach a value close to the emission from galaxies at $z = 7$ would require a very large absorption of Lyα photons by dust in galaxies.

The resulting power spectra of Lyα emission in galaxies and in the IGM obtained with the SimFast21 code are presented in Figure 10 for $z = 7$ and $z = 10$.

We repeated the Lyα power spectra calculation for several redshifts during the EoR and plotted the Lyα power spectra as a function of redshift for several k in Figure 11.

We calculated the intensity of Lyα emission from galaxies and from the IGM (intensities are shown in Figure 12) and found

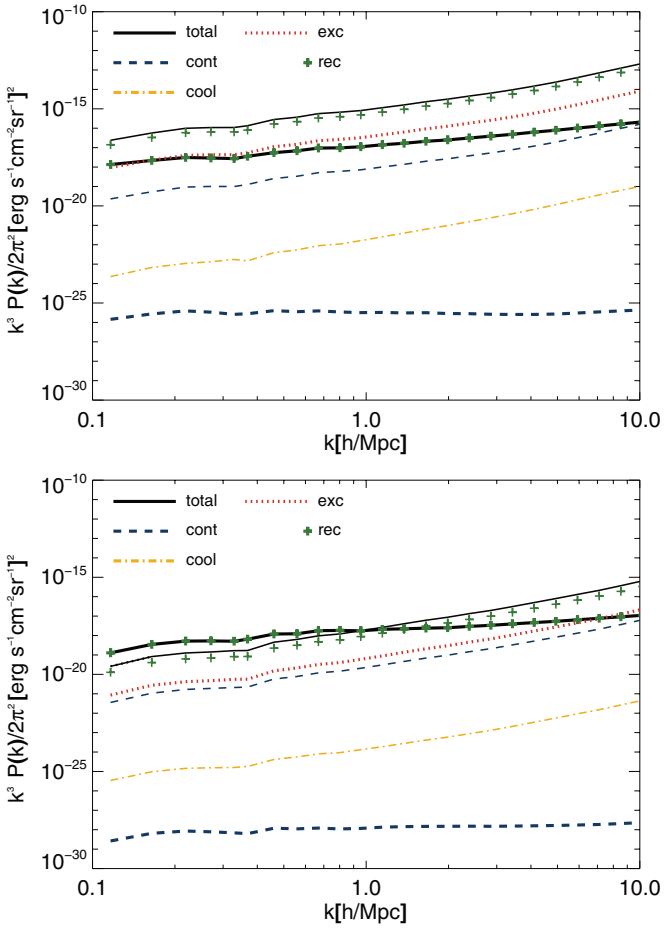

Figure 10. Power spectrum of Lyα surface brightness (νI) from galaxies (thin lines) and from the IGM (thick lines) at redshifts 7 (top) and 10 (bottom). The shown contributions to the Lyα flux are from excitations and collisions, recombinations, continuum emission inside the Lyα width (from galaxies), scattering of Lyn photons (from the IGM), cooling emission in galaxies, and the total emission.

(A color version of this figure is available in the online journal.)

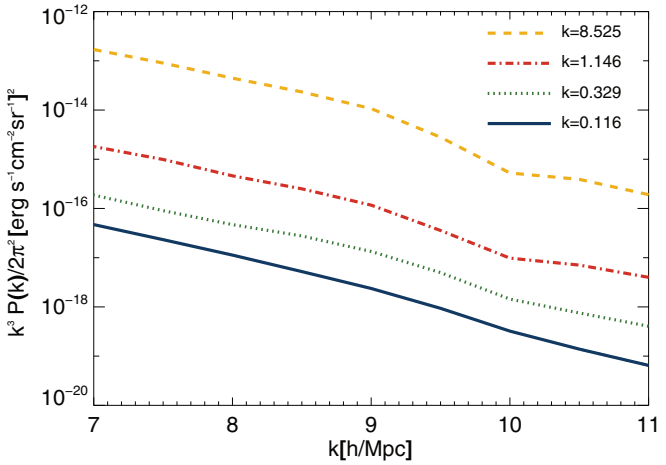

Figure 11. Total power spectrum of Lyα emission during the EoR as a function of redshift.

(A color version of this figure is available in the online journal.)

that, according to our assumptions and as already previously seen, the Lyα emission from galaxies is dominant over the Lyα emission from the IGM at least during the redshift interval from $z = 6$ to $z = 9$.

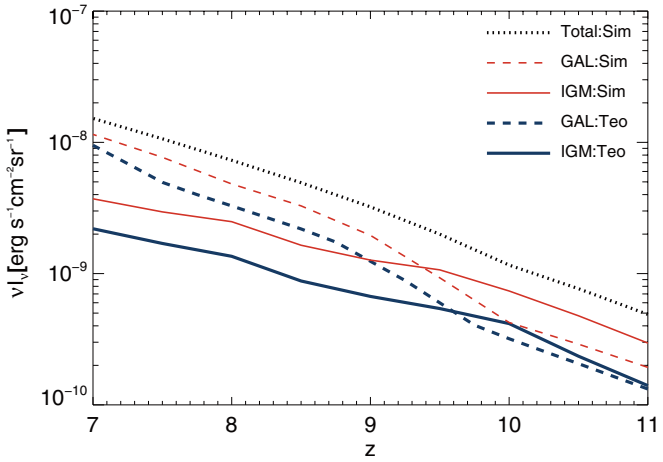

Figure 12. Lyα intensity from galaxies (dashed lines), from the IGM (solid lines) as a function of redshift from our simulation (red thin lines), and from the theoretical calculations (blue thick lines). Also shown is the total Lyα emission from the simulation (dotted line). All the intensities were calculated using the star formation halo mass relation from *Sim1*. The theoretical intensity of Lyα emission from the IGM was calculated using the average IGM ionization values obtained from *Sim1*.

(A color version of this figure is available in the online journal.)

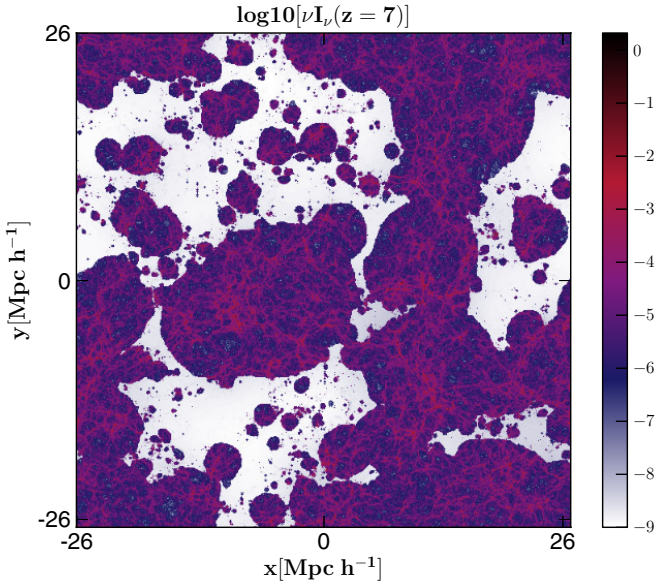

Figure 13. Total Lyα intensity from galaxies and the IGM in erg s^{-1} cm^{-2} sr^{-1} at redshift 7.

(A color version of this figure is available in the online journal.)

Also, a map of the total Lyα intensity in galaxies and in the IGM is presented in Figure 13 for $z = 7$.

Since the star formation halo mass relation is not very constrained, we can use the results obtained with *Sim1* and *Sim3* as the lower and upper bounds to the expected Lyα intensity. The evolution of the Lyα intensity from galaxies, from the IGM, and from galaxies plus IGM can be seen, respectively, in Tables 6, 7, and 8 for simulations *Sim1*, *Sim2*, and *Sim3*.

5. CROSS-CORRELATION BETWEEN Lyα AND 21 cm OBSERVATIONS

Observations of the 21 cm signal from the EoR will suffer from contamination by foregrounds and systematic effects. Since both 21 cm line emission and Lyα line emission trace

Table 6
Surface Brightness (in Observed Frequency times Intensity) in Units of erg s^{-1} cm^{-2} sr^{-1} of Lyα Emission from Galaxies at $z \approx 7$, $z \approx 8$, and $z \approx 10$ for *Sim1*, *Sim2*, and *Sim3*

Simulation	$\nu I_\nu(z=7)$	$\nu I_\nu(z=8)$	$\nu I_\nu(z=10)$
Sim1	1.43×10^{-8}	5.13×10^{-9}	4.55×10^{-11}
Sim2	2.54×10^{-8}	8.34×10^{-9}	5.68×10^{-11}
Sim3	3.57×10^{-8}	1.26×10^{-8}	9.73×10^{-11}

Table 7
Surface Brightness (in Observed Frequency times Intensity) in Units of erg s^{-1} cm^{-2} sr^{-1} of Lyα Emission from the IGM at $z \approx 7$, $z \approx 8$, and $z \approx 10$ for *Sim1*, *Sim2*, and *Sim3*

Simulation	$\nu I_\nu(z=7)$	$\nu I_\nu(z=8)$	$\nu I_\nu(z=10)$
Sim1	4.33×10^{-9}	3.76×10^{-9}	1.74×10^{-9}
Sim2	6.07×10^{-9}	5.17×10^{-9}	2.18×10^{-9}
Sim3	8.53×10^{-9}	7.81×10^{-9}	3.76×10^{-9}

Table 8
Surface Brightness (in Observed Frequency times Intensity) in Units of erg s^{-1} cm^{-2} sr^{-1} of Total Lyα Emission at $z \approx 7$, $z \approx 8$, and $z \approx 10$ for *Sim1*, *Sim2*, and *Sim3*

Simulation	$\nu I_\nu(z=7)$	$\nu I_\nu(z=8)$	$\nu I_\nu(z=10)$
Sim1	1.86×10^{-8}	8.89×10^{-9}	1.79×10^{-9}
Sim2	3.15×10^{-8}	1.35×10^{-8}	2.24×10^{-9}
Sim3	4.42×10^{-8}	2.04×10^{-8}	3.86×10^{-9}

neutral hydrogen, these two lines are expected to be strongly correlated. The cross-correlation of these two lines can be used as an extra method to probe the evolution of the IGM ionized hydrogen fraction. In particular, the power spectra of this cross-correlation will have a discontinuity at a scale that is related to the average bubble size and hence the average ionization fraction in the universe.

During the EoR, the 21 cm signal from galaxies is much smaller than the emission from the IGM, so it is safe to neglect both this galaxy emission and the shot-noise emission in the cross-correlation. Since the Lyα emission from galaxies is dominating over the IGM for most redshifts, we can just concentrate on the Lyα-galaxy/21 cm IGM cross-correlation when analyzing the cross-power spectrum. The cross-correlation between the 21 cm signal and the Lyα line in galaxies is therefore given by

$$P_{\mathrm{Ly}\alpha,21}(z,k) = I_{\mathrm{GAL}} I_{21} \left[P_{\delta\delta} - \frac{1}{1-\bar{x}_i} P_{x_i\delta} \right], \qquad (48)$$

where I_{21} is the average intensity of 21 cm emission, $P_{x_i\delta}(z,k)$ is the cross-correlation power spectra between the ionized field and the matter density fluctuations, $P_{\delta\delta}(z,k)$ is the power spectra of matter density fluctuations, and we are assuming that the Lyα emission is a biased tracer of the underlying dark matter field.

In Figure 14, we show the cross-correlation power spectrum between the total Lyα emission and the 21 cm signal at redshifts 7, 8, 9, and 10. For simulation *Sim1*, these redshifts correspond to ionizing fractions of $x_i = 0.86$, 0.56, 0.35, and 0.23 for redshifts 7, 8, 9, and 10, respectively. In Figure 14, the scale at which $P_{\mathrm{Ly}\alpha,21}(k)$ goes from negative to positive is determined by the average size of the ionized regions. For small scales, the correlation is positive since fluctuations from both lines should be proportional to the underlying density fluctuations, but for large scales (small k), the correlation is negative since the 21 cm line and the Lyα line are characteristic of neutral gas and ionized gas, respectively (and there will be an extra negative contribution from the ionized bubbles).

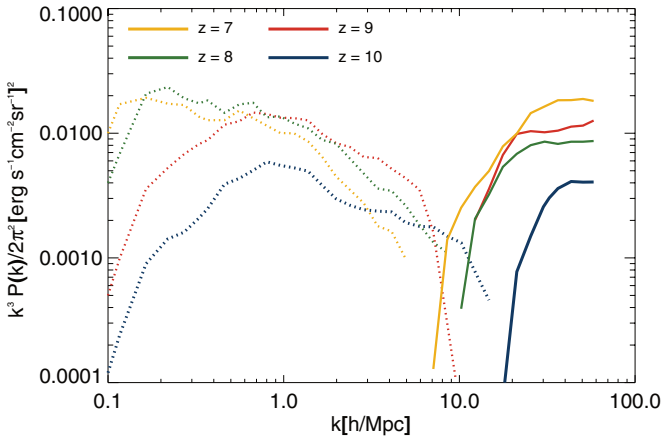

Figure 14. Cross-correlation power spectrum between Lyα emission and the 21 cm signal for redshifts 7, 8, 9, and 10. Dotted lines indicate a negative correlation, and solid lines indicate a positive correlation.
(A color version of this figure is available in the online journal.)

6. OBSERVATIONS

Current observations related to Lyα emission are restricted to narrowband imaging of Lyα emitters during reionization and the direct detection of individual emitters. This has led to order $\sim$200 secure detections at $z > 5$, but systematic uncertainties remain on the fraction that are arising at low redshifts and associated with [O III]/[O II] lines, among others. Due to narrow atmospheric windows, observations in near-IR bands necessary to cover the reionization epoch are also limited to multiple discrete bands. In any case, existing data could be used for a statistical study such as the power spectrum to extract properties of Lyα emitters that remain below the 5σ level of individual source/line identifications. Given that detections do exist at the bright end and our predictions are consistent with the Lyα LFs derived from observational measurements, it is likely that a modest improvement in existing technology and programs will lead to an experiment with sufficient sensitivity to measure the Lyα anisotropy power spectrum during reionization over a broad range of redshifts. The main limitation, unfortunately, is that existing ground-based observations are very limited to small fields of view with narrow bands in the redshift.

Note that from the ground we expect a noise (νI) of $\sim 2.5 \times 10^{-3}$ erg cm^{-2} sr^{-1} (assuming we can avoid the OH lines; otherwise, the intensity will be $\sim 1.0 \times 10^{-1}$ erg cm^{-2} sr^{-1}). From space, the main contamination will be the zodiacal light, which will have a value $\sim 5 \times 10^{-4}$ erg cm^{-2} sr^{-1}. It is possible that a dedicated experiment from the ground can be conceived to improve our understanding of reionization through detailed Lyα mapping over a broad range of redshifts using specific instruments and filters that suppress the atmospheric contamination. Because of this strong atmospheric contamination, sub-orbital and/or orbital experiments may, however, offer a better option. The predictions we have made here can be used as a guide in designing such instruments and experiments.

In Figure 15, we show the expected errors at $z = 7$ (central wavelength of 0.975 μm) for a dedicated compact space-borne template instrument to study Lyα EoR fluctuations. We consider a 20 cm aperture and a spectrometer with resolution

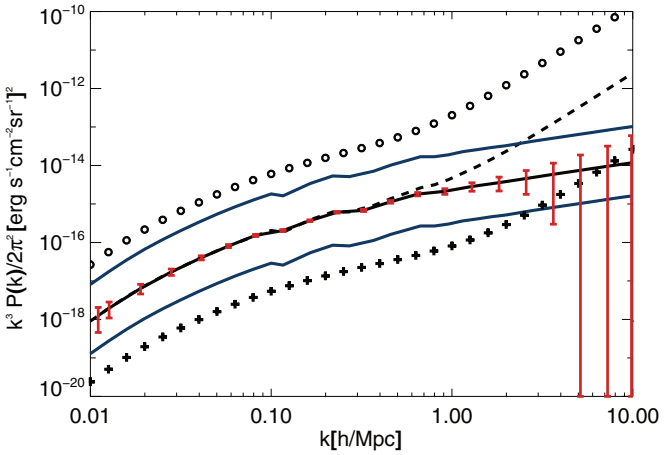

Figure 15. Expected error on the Lyα clustering power spectrum at $z = 7$ using a space-based experiment. Black solid line shows the clustering power spectrum for *Sim3*, while the dashed line includes the shot noise. Red vertical bars show the error. The lower blue solid line shows the clustering power spectrum for *Sim1*, while the top blue solid line shows the same for a model similar to *Sim3* with the same reionization history and optical depth (from *WMAP*) but with an SFR three times larger and a UV escape fraction three times lower, which will generate an Lyα luminosity function larger than what is usually expected at $z = 7$. Circles show the expected Hα power spectrum from $z = 0.5$ that will contaminate the observation, and the crosses give the expected Hα signal after galaxies with an Hα luminosity $>10^{40}$ $L_\odot$ are removed.

(A color version of this figure is available in the online journal.)

$R = \lambda/\Delta\lambda = 200$. The imaging will be done using a 2048 × 2048 HgCdTe detector array in order to cover in one pointing a field of view of 45 × 45 arcmin with a resolution of 10 arcsec pixels on the sky and a spectral range from 0.85 to 1.10 μm. We took a survey area of 20 deg^2 and a total observation time of 2900 hr. This example shows that Lyα EoR science is well within the reach of our modest template instrument. The calculated sensitivities achieved on the deep fields are sufficient to detect Lyα in broad $\Delta k/k$ bins ranging from $k = 0.01$ to 10 h Mpc^{-1} in both clustering and Poisson fluctuations.

Ideally the spectral resolution would match the maximum k available in the angular direction; however, higher spectral resolution requires longer integration times needed to realize photon noise limited sensitivity, which tends to degrade the instrument sensitivity. The angular resolution does not affect surface brightness sensitivity directly, but it does determine the depth to which lower-redshift galaxies may be masked using a deep ancillary continuum galaxy survey. Although the continuum emission from galaxies can in principle be removed by looking at the signal across the frequency direction, as explained before, contamination from other lines at lower redshifts does pose a problem to the detection of the Lyα signal, in particular from the Hα line. The most straightforward way to remove this contamination would be by masking the pixels where these low-z galaxies are found, either from the observation itself or using another, high-sensitivity, continuum observation. For this approach, the angular resolution of the Lyα experiment has to be good enough in order to have enough pixels left after the masking. Therefore, this instrument is required to have higher angular resolution than spectral resolution. Figure 15 also shows the expected contamination from the Hα line from galaxies at $z = 0.5$ (black dots). This was calculated following the same approach as for the Lyα line and using the Hα-to-SFR relation taken from Kennicutt et al. (1994) and Kennicutt (1998b). Removing low-z galaxies down to a mass of $\sim 6.6 \times 10^{10}$ $M_\odot$, corresponding to a cut in luminosity $L > 10^{42}$ erg s^{-1}, would bring this contamination below the Lyα signal (black crosses). Using the Hα LF from Geach et al. (2010) normalized to the SFRD at $z = 0.5$, we get an expected angular density of about 25 Hα emitters per square degree per band, which would mean that only ∼0.98% of the pixels would be masked.

Note that the rejection of interloping low-redshift galaxies requires a full treatment that is beyond the scope of this paper. Foreground rejection may also be significantly enhanced by simultaneously detecting additional EoR spectral features beyond Lyα, which are produced by interlopers with very low probability. Combining these Lyα measurements with other EoR observations (CO, C+, and particularly H I 21 cm) offers additional information on EoR star formation, metallicity, and ionization history. The possibility of constructing an experiment in a near-IR band to measure the Lyα flux in order to correlate it with the 21 cm signal was also explored by Wyithe et al. (2007). Although they used simple models to estimate the fluctuations in each of these two lines, they also considered several foregrounds that will contaminate the observations and concluded that it is possible to remove enough foregrounds that the intensity of radiation emitted from galaxies can be constrained from the cross-correlation.

7. SUMMARY

In this paper, we took into account the main contributions to Lyα emission from recombinations, collisions, continuum emission in galaxies, and scattering of Lyn photons to calculate the intensity of Lyα emission from galaxies and from the IGM during the EoR.

We started by theoretically calculating the intensities using astrophysical data from several observational results and then implemented the calculation in a simulation using a modified version of the code SimFast21 to obtain the spatial fluctuations of Lyα emission. The simulation allowed us to calculate the Lyα emission taking into account the spatial fluctuations of the different astrophysical parameters, which represents an improvement over theoretical calculations that only use the average values.

Our simulations showed that to achieve optical depths compatible with the *WMAP* constraints, the high SFRD required implies that for reasonable values of UV and Lyα escape fraction the intensity of Lyα emission from galaxies is dominant over the emission from the IGM.

By testing different SFR halo mass parameterizations, we constrained the intensity of Lyα emission from galaxies to be about (1.43–3.57) × 10^{-8} and (4.55–9.73) × 10^{-11} erg^{-1} cm^{-2} sr^{-1} at redshifts 7 and 10, respectively, which is dominant over the intensity of Lyα emission from the IGM at $z = 7$ (about 1.6×10^{-5}) but less at $z = 10$ (1.1×10^{-10} erg s^{-1} cm^{-2} sr^{-1}). Since the intensity levels we found are lower than the extragalactic background intensity from galaxies and so are too low to be detected with an experiment aiming the absolute background intensity, we propose an intensity mapping experiment that will allow us to measure the Lyα power spectrum.

For reasonable astrophysical conditions the process of hydrogen reionization was done by UV radiation originated in galaxies with luminosities below the high-redshift observational threshold. In this work, we showed the different ways by which UV emission is connected to Lyα emission, and so we stress how

it would be useful to use intensity mapping of Lyα emission to probe the overall intensity of UV radiation.

Lyα emission can also be connected to the 21 cm signal from the EoR, since the continuum photons above the Lyα line that redshift to this line in the IGM contribute to the radiative coupling of the 21 cm signal to the gas temperature. The cross-correlation of the Lyα and the 21 cm lines can be used to reduce systematics and foregrounds encountered with 21 cm observations. In particular, the discontinuity of the cross-correlation power spectra will provide constraints in the evolution of the IGM ionized fraction.

In previous studies, we have discussed the use of CO molecular and C II fine-structure atomic lines to complement 21 cm data in the attempt to probe the IGM during reionization. Our study shows that Lyα intensity mapping is also a viable approach to probe reionization and is within experimental reach over the coming decade.

This work was supported by FCT-Portugal with the grant SFRH/BD/51373/2011 for M.B.S. and under grant PTDC/FIS/100170/2008 for M.B.S. and M.G.S.

A.C. and Y.G. acknowledge support from NSF CAREER AST-0645427 and NASA NNX10AD42G at UCI.

M.B.S. was a long-term Visiting Student at UCI, supported by NSF CAREER AST-0645427, when this work was initiated, and she thanks the Department of Physics and Astronomy at UCI for hospitality during her stay.

REFERENCES

Barkana, R., & Loeb, A. 2001, PhR, 349, 125
Barkana, R., & Loeb, A. 2005, ApJ, 626, 1
Bouwens, R. J., Illingworth, G. D., Labbe, I., et al. 2011, Natur, 469, 504
Bouwens, R. J., Illingworth, G. D., Oesch, P. A., et al. 2012a, ApJL, 752, 5
Bouwens, R. J., Illingworth, G. D., Oesch, P. A., et al. 2012b, ApJ, 754, 83
Boylan-Kolchin, M., Springel, V., White, S. D. M., Jenkins, A., & Lemson, G. 2009, MNRAS, 398, 1150
Brown, R. L., & Mathews, W. G. 1970, ApJ, 160, 939
Cantalupo, S., Porciani, C., & Lilly, S. J. 2008, ApJ, 672, 48
Chen, X., & Miralda-Escudé, J. 2008, ApJ, 684, 18
Chuzhoy, L., & Zheng, Z. 2007, ApJ, 670, 912
Conroy, C., & Wechsler, R. H. 2009, ApJ, 696, 620
Cooray, A., Gong, Y., Smidt, J., & Santos, M. G. 2012, ApJ, 756, 92
Davé, R., Cen, R., Ostriker, J. P., et al. 2001, ApJ, 552, 473
Dayal, P., Ferrara, A., & Saro, A. 2010, MNRAS, 402, 1449
De Lucia, G., & Blaizot, J. 2007, MNRAS, 375, 2
Dijkstra, M., Haiman, Z., & Spaans, M. 2006a, ApJ, 649, 14
Dijkstra, M., Haiman, Z., & Spaans, M. 2006b, ApJ, 649, 37
Dopita, M. A., & Sutherland, R. S. 2003, Astrophysics of the Diffuse Universe (Berlin: Springer)
Fan, X., Strauss, M. A., Becker, R. H., et al. 2006, AJ, 132, 117
Fardal, M. A., Katz, N., Gardner, J. P., et al. 2001, ApJ, 562, 605
Fernandez, E. R., & Komatsu, E. 2006, ApJ, 646, 703
Fernández-Soto, A., Lanzetta, K. M., & Chen, H.-W. 2003, MNRAS, 342, 1215
Forero-Romero, J. E., Yepes, G., Gottlöber, S., et al. 2011, MNRAS, 415, 3666
Furlanetto, S. R., Oh, S. P., & Briggs, F. H. 2006, PhR, 433, 181
Geach, J. E., Cimatti, A., Percival, W., et al. 2010, MNRAS, 402, 1330
Gnedin, N. Y., Kravtsov, A. V., & Chen, H.-W. 2008, ApJ, 672, 765
Gong, Y., Cooray, A., Silva, M., et al. 2012, ApJ, 745, 49
Gong, Y., Cooray, A., Silva, M. B., Santos, M. G., & Lubin, P. 2011, ApJL, 728, 46
Gould, A., & Weinberg, D. H. 1996, ApJ, 468, 462
Guo, Q., White, S., Boylan-Kolchin, M., et al. 2011, MNRAS, 413, 101
Haardt, F., & Madau, P. 2012, ApJ, 746, 125
Haiman, Z., Spaans, M., & Quataert, E. 2000, ApJL, 537, 5
Hayes, M., Schaerer, D., Östlin, G., et al. 2011, ApJ, 730, 8
Iye, M., Ota, K., Kashikawa, N., et al. 2006, Natur, 443, 186
Jensen, H., Laursen, P., Mellema, G., et al. 2013, MNRAS, 428, 1366
Jiang, L., Egami, E., Kashikawa, N., et al. 2011, ApJ, 743, 65
Karzas, W. J., & Latter, R. 1961, ApJS, 6, 167
Kashikawa, N., Shimasaku, K., Malkan, M. A., et al. 2006, ApJ, 648, 7
Kennicutt, R. C., Jr. 1998a, ARA&A, 36, 189
Kennicutt, R. C., Jr. 1998b, ApJ, 498, 541
Kennicutt, R. C., Jr., Tamblyn, P., & Congdon, C. E. 1994, ApJ, 435, 22
Komatsu, E., Smith, K. M., Dunkley, J., et al. 2011, ApJS, 192, 18
Larson, D., Dunkley, J., Hinshaw, G., et al. 2011, ApJS, 192, 16
Latif, M. A., Schleicher, D. R. G., Spaans, M., & Zaroubi, S. 2011, MNRAS, 413, L33
Lehnert, M. D., Nesvadba, N. P. H., Cuby, J.-G., et al. 2010, Natur, 467, 940
Lidz, A., Furlanetto, S. R., Oh, S. P., et al. 2011, ApJ, 741, 70
Madau, P., & Pozzetti, L. 2000, MNRAS, 312, L9
Maraston, C. 2005, MNRAS, 362, 799
Martin, P. G. 1988, ApJS, 66, 125
Mesinger, A., & Furlanetto, S. 2007, ApJ, 669, 663
Mesinger, A., & Haiman, Z. 2007, ApJ, 660, 923
Mitra, S., Choudhury, T. R., & Ferrara, A. 2012, MNRAS, 419, 1480
Oesch, P. A., Bouwens, R. J., Illingworth, G. D., et al. 2012, ApJ, 745, 110
Ota, K., Iye, M., Kashikawa, N., et al. 2008, ApJ, 677, 12
Ota, K., Iye, M., Kashikawa, N., et al. 2010, ApJ, 722, 803
Ouchi, M., Shimasaku, K., Akiyama, M., et al. 2008, ApJS, 176, 301
Ouchi, M., Shimasaku, K., Furusawa, H., et al. 2010, ApJ, 723, 869
Pawlik, A. H., Schaye, J., & van Scherpenzeel, E. 2010, in ASP Conf. Ser. 432, New Horizons in Astronomy: Frank N. Bash Symposium 2009, ed. L. M. Stanford, J. D. Green, L. Hao, & Y. Mao (San Francisco, CA: ASP), 230
Pengelly, R. M. 1964, MNRAS, 127, 145
Popesso, P., Biviano, A., Rodighiero, G., et al. 2012, A&A, 537, A58
Razoumov, A. O., & Sommer-Larsen, J. 2010, ApJ, 710, 1239
Salvaterra, R., Della Valle, M., Campana, S., et al. 2009, Natur, 461, 1258
Santos, M. G., Ferramacho, L., Silva, M. B., Amblard, A., & Cooray, A. 2010, MNRAS, 406, 2421
Santos, M. G., Silva, M. B., Pritchard, J. R., Cen, R., & Cooray, A. 2011, A&A, 527, A93
Santos, M. R. 2004, MNRAS, 349, 1137
Schaerer, D. 2002, A&A, 382, 28
Sheth, R. K., & Tormen, G. 1999, MNRAS, 308, 119
Shibuya, T., Kashikawa, N., Ota, K., et al. 2012, ApJ, 752, 114
Shimasaku, K., Kashikawa, N., Doi, M., et al. 2006, PASJ, 58, 313
Shull, J. M., & van Steenberg, M. E. 1985, ApJ, 298, 268
Shull, M., Harness, A., Trenti, M., & Smith, B. 2012, ApJ, 747, 100
Siana, B., Teplitz, H. I., Colbert, J., et al. 2007, ApJ, 668, 62
Smith, B. D., Hallman, E. J., Shull, J. M., & O'Shea, B. W. 2011, ApJ, 731, 6
Springel, V., White, S. D. M., Jenkins, A., et al. 2005, Natur, 435, 629
Steidel, C. C., Bogosavljević, M., Shapley, A. E., et al. 2011, ApJ, 736, 160
Taniguchi, Y., Ajiki, M., Nagao, T., et al. 2005, PASJ, 57, 165
Visbal, E., & Loeb, A. 2010, JCAP, 11, 16
Wang, X., Tegmark, M., Santos, M. G., & Knox, L. 2006, ApJ, 650, 529
Wise, J. H., & Cen, R. 2009, ApJ, 693, 984
Wyithe, S., Loeb, A., & Schmidt, B. 2007, arXiv:0705.1825
Yajima, H., Choi, J.-H., & Nagamine, K. 2011, MNRAS, 412, 411
Zahn, O., Reichardt, C. L., Shaw, L., et al. 2012, ApJ, 756, 65
Zaldarriaga, M., Colombo, L., Komatsu, E., et al. 2008, arXiv:0811.3918
Zheng, Z., Cen, R., Trac, H., & Miralda-Escudé, J. 2010, ApJ, 716, 574
Zheng, Z., Cen, R., Weinberg, D., Trac, H., & Miralda-Escudé, J. 2011, ApJ, 739, 62